LITHOS 530-531 (2026) 108485

Contents lists available at ScienceDirect

LITHOS

journal homepage: www.elsevier.com/locate/lithos

Transformation of calcite-bearing ijolites to biotite calcite carbonatites – A case study from Dicker Willem, southern Namibia

Lorenz Kemmler [a,b,*], R. Johannes Giebel [b,c], Benjamin F. Walter [a], Michael A.W. Marks [a], David L. Reid [d], Mohsin Raza [e,f], Tobias Kluge [e], Gregor Markl [a]

[a] Eberhard Karls University Tübingen, Department for Petrology and Mineral Resources, Schnarrenbergstraße 94-96, 72076 Tübingen, Germany
[b] Technical University Berlin, Department of Applied Geochemistry, Ernst-Reuter-Platz 1, 10587 Berlin, Germany
[c] University of the Free State, Department of Geology, 250 Nelson-Mandela-Drive, Bloemfontein 9300, South Africa
[d] University of Cape Town, Department of Geological Sciences, 13 University Avenue South, Rondebosch 7701, South Africa
[e] Karlsruhe Institute of Technology, Chair of Economic Geology and Geochemistry, Adenauerring 20b, 76131 Karlsruhe, Germany
[f] Department of Geology, Bacha Khan University Charsadda, Pakistan

ARTICLE INFO

Keywords:
Carbonatite
Fenitization
Metasomatism
Ijolite
Silicocarbonatite

ABSTRACT

The Eocene Dicker Willem carbonatite complex (southern Namibia) primarily comprises fine-grained calcite carbonatites hosting xenoliths and irregular inclusions of calcite ijolites, calcite syenites, nepheline silicocarbonatites, and coarse-grained calcite carbonatites. A 7 by 6 m xenolith within the complex exhibits zonal lithological transitions, evolving from calcite-bearing ijolite via calcite syenite and silicocarbonatite to coarse-grained calcite carbonatite.

This succession reflects initial carbohydrothermal alteration (fenitization), followed by interaction with carbonatitic melt, as evidenced by textures, mineralogy and element transport. In the central ijolitic zone, primary nepheline is replaced by orthoclase, while the outer margins show intense resorption of original silicate minerals, replaced by coarse calcite, biotite ± aegirine-rich clinopyroxene and magnetite, ultimately forming coarse calcite carbonatite.

Mass transfer reveals enrichment in Ca, Sr, and REE, alongside depletion in Na, Mg, Al, Si, and K. Sample sets from other parts of Dicker Willem, transitioning from ijolite to nepheline silicocarbonatite, exhibit increasing replacement of nepheline by cancrinite, driven by magmatic interaction as well.

These findings indicate that nepheline silicocarbonatite is a transitional lithology, not an orthomagmatic rock, formed through in-situ dissolution-reprecipitation of silicates and replacement by calcite, with significant silica introduction into the carbonatitic magma. Scaling this process up to the entire Dicker Willem Complex suggests that even silicate-bearing coarse-grained calcite carbonatites could result from carbonatite magma-induced transformation, consistent with published isotopic and mineral data.

1. Introduction

Primary carbonatites are rare igneous rocks with at least 454 (Schmidt et al., 2024) confirmed occurrences worldwide (out of >600 previously alleged occurrences), that contain >50 to arguably >25 modal% carbonate minerals (mostly calcite and/or dolomite, Le Maitre et al., 2002; Mitchell, 2005; Tappe and Mitchell, 2026). Other minerals such as apatite, magnetite, clinopyroxene or mica can occur in significant amounts in addition to mostly accessory REE and other HFSE minerals (e.g., bastnäsite, monazite, strontianite or pyrochlore).

Most carbonatites occur in close spatial association with a variety of silicate rocks, forming diverse carbonatite–silicate rock assemblages. A widely accepted explanation is that these associations derive from a common parental melt extracted from sublithospheric sources (e.g., Yaxley et al., 2022). Mainly based on experimental work, proposed models for the formation of carbonatite melts include (1) low-grade partial melting of carbonate-bearing mantle domains (Harmer and Gittins, 1998; Wallace and Green, 1988), (2) segregation from CO_2-bearing and SiO_2-undersaturated magma by fractional crystallization (Watkinson and Wyllie, 1971), (3) liquid immiscibility (Brooker and

* Corresponding author at: Eberhard Karls University Tübingen, Department for Petrology and Mineral Resources, Schnarrenbergstraße 94-96, 72076 Tübingen, Germany.
E-mail address: lorenz.kemmler@gmail.com (L. Kemmler).

https://doi.org/10.1016/j.lithos.2026.108485
Received 8 August 2025; Received in revised form 2 March 2026; Accepted 3 March 2026
Available online 7 March 2026

Kjarsgaard, 2011; Lee and Wyllie, 1998) or combinations thereof. The significance of these processes and their applicability to nature, however, are the subject of heated debates (Gittins and Mitchell, 2023; Mitchell and Gittins, 2022; Schmidt et al., 2024 and references therein).

The subsequent evolution of carbonatitic magmas involves low-pressure fractional crystallization towards so-called brine-melts and late-stage transformation into more conventional carbohydrothermal fluids forming rocks termed carbothermalites (Mitchell and Gittins, 2022; Walter et al., 2021; Yuan et al., 2023). Carbonatitic magmas consistently coexist with immiscible, alkali-rich aqueous fluids (Guzmics et al., 2019), while their exact composition is highly variable and can evolve during subsequent magmatic stages (Le Bas, 2008; Walter et al., 2021). These fluids may interact with the surrounding host rocks generating prominent aureoles of metasomatised rocks called fenites (Le Bas, 2008), with the typical minerals including albite, orthoclase, sodic clinopyroxene (aegirine), amphibole (e.g., arfvedsonite, riebeckite) and others (reviewed in Elliott et al., 2018). Carbonatite magmas can also directly interact with crustal host rocks and xenoliths, which leads to formation of Fe—Mg silicate minerals, such as olivine, clinopyroxene, and mica (e.g., Anenburg and Mavrogenes, 2018; Giebel et al., 2019b; Chmyz et al., 2022; Vasyukova and Williams-Jones, 2022; Su et al., 2023; Walter et al., 2022). On a larger scale, such interaction might result in an outward zonation of carbonate-bearing silicate rocks around carbonatite bodies, including dunite, peridotite, pyroxenite, ijolite, syenite, glimmerite and others, as recently proposed for carbonatite complexes like Palabora, Jacupiranga or Kovdor (Chmyz et al., 2022; Gudelius et al., 2023; Vasyukova and Williams-Jones, 2022).

Carbonatites exceeding 20 wt.% of SiO_2 are generally defined as silicocarbonatites (Le Maitre et al., 2002) with the major non-carbonate minerals being used as mineralogical prefixes (e.g., nepheline silicocarbonatite) for further subdivision. Silicocarbonatites are believed to form by different processes:

(1) They are suggested to represent either a parental silica-bearing carbonate melt or a transitional (hybrid) magma derived from a carbonated silicate melt through silicate mineral fractionation. These melts may finally evolve into "pure" carbonatite melts via fractionation producing silicate cumulates of silicocarbonatite compositions, or separate into carbonatite-silicate magma pairs by immiscibility (e.g., Cooper and Reid, 1998; Doroshkevich et al., 2017; Moore et al., 2022; Savard and Mitchell, 2021). (2) The most recent hypothesis includes the contamination/assimilation of carbonatite melts by silicate rocks (wall-rocks and xenoliths), which ensures a successive/sequential introduction of silica to form appropriate amounts of silicates in a carbonatitic system (e.g., Anenburg and Walters, 2024; Chmyz et al., 2025; Giebel et al., 2019b; Vasyukova and Williams-Jones, 2022; Vuorinen and Skelton, 2004; Walter et al., 2022).

The present study identifies an additional mechanism for silicocarbonatite formation, characterised by magmatic transformation of silicate rocks through interaction with carbonatite magma. The process involves in-situ dissolution, resorption and displacement of the initial mineral assemblage (clinopyroxene, nepheline, orthoclase and andradite) and (re-)precipitation of calcite, clinopyroxene, biotite and magnetite.

To investigate this interaction between precursor calcite ijolite, carbohydrothermal fluids and carbonatite magma, we focus on a 7 by 6 m large xenolith set in a matrix of fine-grained calcite carbonatite from the Dicker Willem carbonatite in Namibia. A succession of events involving fluid-induced and melt-induced processes is proposed, leading to the formation of a whole array of unusual rock types ranging from calcite-bearing ijolites and calcite syenites, via clinopyroxene-bearing silicocarbonatites to coarse biotite calcite carbonatites on the outcrop scale – each representing different flavours and variable progression of a common rock-fluid-melt interaction process. Our findings contribute to the current debate on silicate-carbonatite rock associations and silicocarbonatite formation in general. For the studied locality, our new data prompted re-evaluation of previous interpretations on the significance of silicocarbonatites and its applicability can be tested on other carbonatite occurrences.

2. Geological context

The Dicker Willem complex (also known as Dikwillem or Garub mountain) in southern Namibia is situated approx. 90 km east of Lüderitz exposed as a 600 m elevated "inselberg" with a diameter of about 2.5 km (Figs. 1 & 2A). The complex intruded into Proterozoic (1.1 Ga) basement gneisses of the Namaqua-Natal-Metamorphic Complex (Aus-Domain; Cooper, 1988; Macey et al., 2022) and was dated to an Eocene age of 49 ± 1 Ma (K—Ar on biotite and Rb—Sr on biotite and carbonate; Reid et al., 1990). It was suggested that the Dicker Willem Complex is part of an age-progressive volcanic track trending roughly northeast to southwest as one of the various alkaline magmatic lineaments crossing the southwestern continental margin of Africa (Ogungbuyi, 2020; Reid, 1991). Alternatively, the Dicker Willem Complex may be assigned (on a regional scale) to the structurally controlled Kudu Lineament-related magmatic complexes (Kieshöhe, Kaukausib, Teufelskuppe and Karingarab; Walter et al., 2022) to be distinguished from the Lüderitz Alkaline Province (~130 Ma, Marsh, 1975; Reid et al., 1990).

The Dicker Willem complex primarily consists of brown fine-grained calcite carbonatite (FGCC), also referred to as alvikite (Cooper, 1988). It comprises assemblages of multiple intrusions of sheets, dykes, pipes, pods and veins with complex crosscutting relations. These FGCCs intruded into white coarse-grained calcite carbonatite (CGCC), formerly sövite, forming discontinuous cone sheets, ring dykes, with irregular enclaves and xenoliths of CGCC within (Fig. 2E), as well as late carbonatite breccia vents at the centre (Cooper, 1988). During emplacement, the surrounding granite gneisses underwent fenitization, resulting in both potassic and sodic varieties (Cooper and Reid, 2000). Minor peripheral trachytes and trachyte breccias occur as radial dykes, plugs, sills and cone sheets, believed to be formed by melting from high grade fenite and thus a genetically unrelated, but contemporaneous immiscible magma (Cooper and Reid, 2000). The entire sequence is crosscut by ferro-carbonatite which appear as diatreme breccias, tuff pipes, dykes and veins.

Xenoliths (up to tens of meters in size) of partly carbonate-bearing clinopyroxene-nepheline ± orthoclase-rocks within CGCC have been interpreted as disrupted remnants of an early magmatic ijolite-syenite suite (Cooper, 1988). Finer-grained, textually distinct, equigranular carbonate-rich sections represent compositional transitions between the ijolite-syenite suite and the CGCC. These so-called nepheline silicocarbonatites (previously termed nepheline sövites) are interpreted as a parental magma capable of co-precipitating calcite and silicates, forming calcite carbonatites and ijolite cumulates through gravity settling (Cooper and Reid, 1998).

In summary, the following sequence of events was proposed: (1) emplacement of calcite ijolite, (2) intrusion of CGCC causing disruption of calcite ijolite at depth, (3) intrusion of trachyte, (4) emplacement of FGCC disrupting CGCC, (5) intrusion of ferro-carbonatite dykes and formation of steep-sided, funnel-shaped ferro-carbonatitic breccia or tuff pipes in the near the summit of the complex (Cooper, 1988).

3. Material and methods

3.1. Sample material

During field work in 2019, a large xenolith (about 5 × 9 m in size) exposed on the northern edge of the Dicker Willem complex (location DW002; −26°27′28.9"N, 16°00′57.8″E, WGS84 33 J, Fig. 1) was systematically sampled along a profile (A to H) from the centre of the xenolith into the host FGCC (Figs. 2B-D). For comparison, proximate FGCC 15 m SE (DW003) and syenite 35 m SE (DW004) and more distant CGCC 60 m SE (DW005) and 200 m S (DW010) of the xenolith were sampled (Fig. 1). Ijolite, nepheline silicocarbonatite and coarse-grained

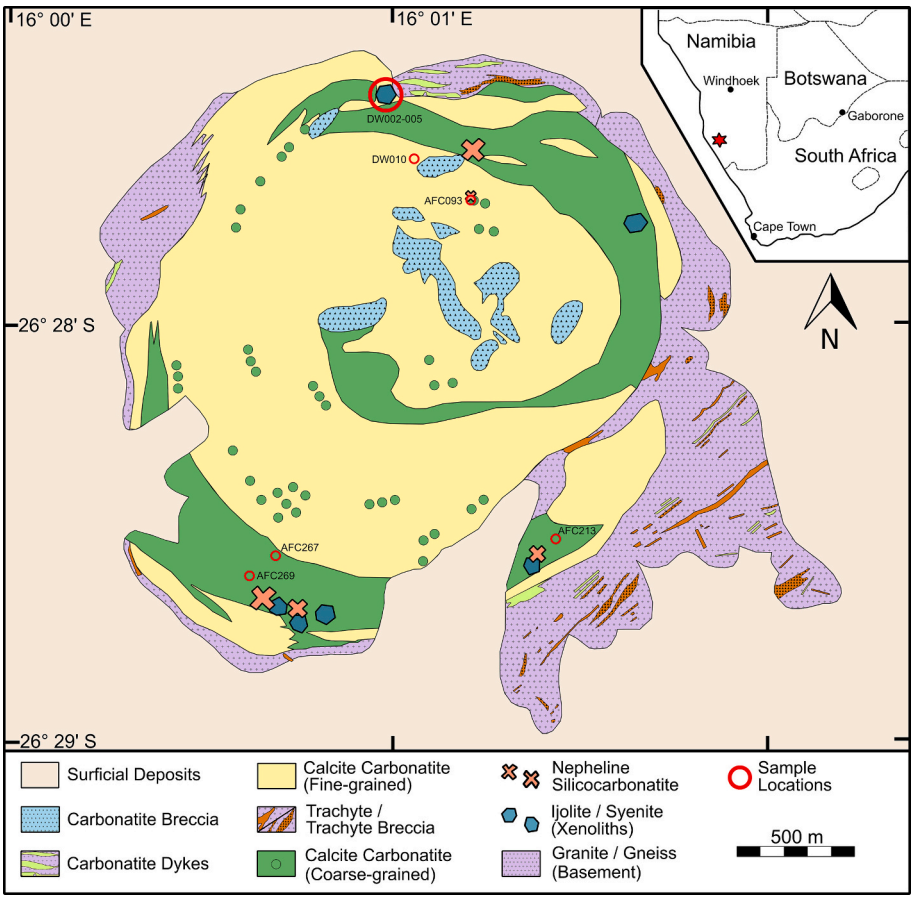

Fig. 1. Geological map of the Dicker Willem Complex (modified after Cooper and Reid, 1998), with occurrences of nepheline silicocarbonatite (orange crosses), ijolite-syenite (blue polygons) and enclaves of coarse-grained calcite carbonatite within the main fine-grained calcite carbonatite (green dots, not to scale). The location of the studied xenolith is marked with a red circle at the northern flank of the intrusion, and other sample localities marked as well. (For interpretation of the references to colour in this figure legend, the reader is referred to the web version of this article.)

calcite carbonatite from the southern part of the complex sampled during field campaigns in 1987 and 1994 (samples AFC093, AFC213, AFC267, AFC268, AFC269) were studied for comparison, summing up to a total of 26 samples (Table 1).

3.2. Petrographic and mineralogical analysis

The samples were examined using transmitted light microscopy, scanning electron microscopy (SEM, Phenom XL and TM3030+, Tübingen), and by micro x-ray fluorescence analysis (μ-XRF, M4 Tornado Bruker AXS, Berlin). The SEM instruments, Phenom XL and TM3030+, differ in their detector configurations and analytical capabilities: the Phenom XL features a larger sample chamber and automated functions for detailed analysis, while the TM3030+ offers a compact design optimised for rapid imaging. Both instruments operated at an acceleration voltage of 15 kV, utilizing backscattered electron (BSE) imaging to enhance compositional contrast, along with elemental mapping and spot analyses for geochemical characterization.

For μ-XRF, the X-ray beam is generated from a Rh tube with an acceleration voltage of 50 kV and a beam current of 600 μA. The measuring point distance was 20 μm at 20 μm beam diameter and a measuring time of 30 ms per analysis spot using the area mode. The mappings were evaluated with the internal software M4 Tornado (Bruker). To determine the modal mineralogy of the samples from combined element maps, the phase evaluation mode was used. In addition, distinct areas of single minerals were selected to obtain semiquantitative analysis of their mineral compositions.

3.3. Whole rock geochemistry

Whole-rock major element geochemistry was determined by wavelength dispersive X-ray fluorescence (WD-XRF-S4 Explorer, Bruker AXS) on fused beads (Li-tetraborate/−metaborate: sample ratio of 10:1) at the Laboratory for Environmental and Raw Material Analysis (LERA, KIT, Karlsruhe). The accuracy (between 1 and 6%) was monitored using certified reference materials (JDO-1, SY-2, PCC-1, SARM 5, RGM-1, AGV-1). Sulfur and carbon analyses were performed using a Carbon-Sulfur-Analyser CS-2000 (ELTRA). The accuracy (<0.2%) and reproducibility (<6%) were verified by correlation with certified reference materials (steel, barium sulfate). Trace elements were determined by ICP-MS (iCAP RQ, Thermo Fisher Scientific) after HNO_3-HF-$HClO_4$-HCl acid digestion of the powdered sample (100 mg). To ensure complete silicate decomposition, 40% HF (supra pure), 65% $HClO_4$ (normatom) and the pre-oxidised (65% HNO_3, subboiled) sample were heated in a closed Teflon vessel for 16 h at 120 °C. After evaporating the acids to incipient dryness, the residue was re-dissolved in 65% HNO_3 (subboiled) and HCl (30% normatom) and then evaporated three times to ensure purification. The final residue was redissolved in 50 ml of ultrapure water. The precision of the ICP-MS measurement was in the range of 1%. Measurements were regularly checked using a 5 μg/l standard solution. The precision and accuracy of the entire method including acid digestion were monitored by including certified reference materials CRM-Sy2 and GRE-03 (High-Purity Standards, Inc.) in the measurement sequence every ten samples (SD is between 1% and 8% for most elements).

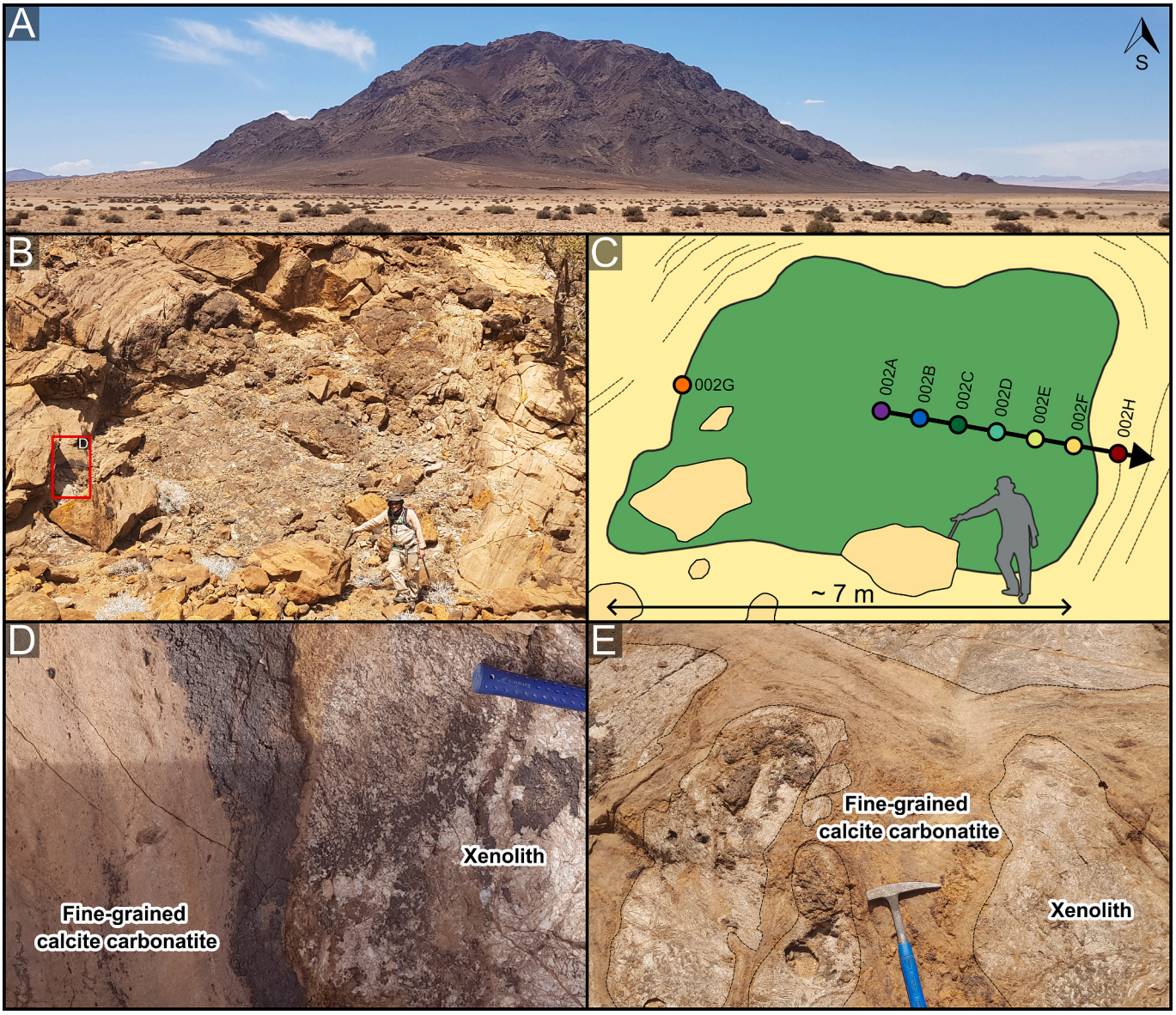

Fig. 2. Field aspects of the Dicker Willem Complex (Namibia). A) View towards the northern flank of the complex. B) Photograph of the studied xenolith, with small red inlier showing position of D. C) Schematic sketch of B, with sample localities of DW002A-H. D) Photograph of the contact between the xenolith and the FGCC with a dark ferroan dolomite layer in between. E) Enclaves of coarse-grained calcite carbonatite (CGCC) within fine-grained calcite carbonatite (FGCC). (For interpretation of the references to colour in this figure legend, the reader is referred to the web version of this article.)

3.4. Mineral compositions

Electron probe micro-analysis (EPMA) of clinopyroxenes was conducted using a JEOL JXA-8230 microanalyzer at the Department of Geosciences, University of Tübingen, operated in wavelength-dispersive mode. The analyses were performed at an acceleration voltage of 15 kV and a beam current of 20 nA. The peak count times were set to 10 s for light and volatile elements to prevent the loss of alkalis during the measurement process, 16 s for major elements and extended to 30 s for trace elements, with background measurement times being half of the respective peak count times. Calibration was achieved using a combination of synthetic and natural standards. An internal φ(ρz) correction was utilised for raw data processing. Specific details of the analytical protocols are provided in the supplementary data. Mineral formula calculations based on 6 anions were conducted, and the determination of Fe^{2+} and Fe^{3+} in clinopyroxene was carried out to maintain charge balance, assuming an ideal lattice site occupancy of 4 cations per formula unit.

3.5. Carbon and oxygen stable isotopes

Powdered carbonatite samples were analysed for their stable isotope ratios ($\delta^{13}C$, $\delta^{18}O$) considering their mixed nature (0–80% calcite and 20–100% dolomite/ankerite component). The sample sizes for isotope analyses were adjusted that the pure carbonate fraction provides a sample signal comparable to the reference gas signal (corresponding to >40 μg C). Following Al-Aasm et al. (1990) and Baudrand et al. (2012), we analysed carbonate fractions without prior separation by leveraging the different reaction rates of calcite and other carbonates with phosphoric acid. Calcite was fully reacted at 25 °C within 2 h, while residual carbonates were allowed to react at 50 °C for 24 h after an intermediate flushing step.

Carbonate samples were reacted in glass vials of a Gas Bench II system heated to 25 and 50 °C (depending on carbonate fraction of interest). Prior to reaction the samples were flushed with He and 10 acid drops were injected afterwards manually by a syringe. The evolving CO_2 was flushed to the Delta V Advantage IRMS with a He flow after 2 h at

Table 1
Sample list, with current and old rock classification, location and applied methods (WR - whole rock; µXRF - micro X-ray fluorescence; CO - C and O stable isotopes; EPMA – Electron probe micro analyser).

Sample	Rock type current classification theme	Rock type sensu Cooper, 1988	Locality	Applied Methods
DW002A	Ijolite (xenolith)	Ijolite	26°27′28.9″S, 16°00′57.8″E	petrography, WR, µXRF, CO, EPMA
DW002B	Ijolite (xenolith)	Ijolite	26°27′28.9″S, 16°00′57.8″E	petrography, WR, µXRF
DW002C	Syenite (xenolith)	Syenite	26°27′28.9″S, 16°00′57.8″E	petrography, WR, µXRF, CO
DW002D	Syenite (xenolith)	Syenite	26°27′28.9″S, 16°00′57.8″E	petrography, WR, µXRF, CO, EPMA
DW002E	Coarse-grained calcite carbonatite (xenolith)	Sövite	26°27′28.9″S, 16°00′57.8″E	petrography, WR, µXRF, CO, EPMA
DW002F	Coarse-grained calcite carbonatite (xenolith)	Sövite	26°27′28.9″S, 16°00′57.8″E	petrography, WR, µXRF, CO, EPMA
DW002G	Fine-grained calcite carbonatite (contact)	Alvikite	26°27′28.9″S, 16°00′57.8″E	petrography, µXRF
DW002H	Fine-grained calcite carbonatite (host rock)	Alvikite	26°27′28.9″S, 16°00′57.8″E	petrography, WR, µXRF, CO
DW003	Fine-grained calcite carbonatite	Alvikite	26°27′28.9″S, 16°00′58.1″E	petrography, WR, µXRF
DW004	Syenite	Syenite	26°27′29.4″S, 16°00′59.9″E	petrography, WR, µXRF
DW005	Coarse-grained calcite carbonatite	Sövite	26°27′34.1″S 16°00′58.9″E	petrography, WR
DW010	Fine-grained calcite carbonatite	Alvikite	26°27′34.1″S 16°00′58.9″E	petrography, WR
AFC093A	Ijolite	Ijolite	26°27′44.3″S, 16°01′11.2″E	petrography
AFC093B-F	Nepheline silicocarbonatite	Nepheline Sövite	26°27′44.3″S, 16°01′11.2″E	petrography, µXRF
AFC213	Coarse-grained calcite carbonatite cumulate	Sövite Cumulate	26°28′34.7″S, 16°01′24.0″E	petrography, µXRF
AFC267A-C	Ijolite/Nepheline silicocarbonatite	Urtite/ Nepheline Sövite	26°28′36.3″S, 16°00′41.0″E	petrography
AFC268A-B	Ijolite/Nepheline silicocarbonatite	Urtite/ Nepheline Sövite	26°28′38.5″S, 16°00′39.5″E	petrography
AFC269A-C	Ijolite/Nepheline silicocarbonatite	Ijolite/ Nepheline Sövite	26°28′40.8″S, 16°00′38.5″E	petrography

25 °C (calcite) and 24 h at 50 °C (other carbonates). Each sample gas was analysed in 10 acquisitions. A measurement sequence included a background analysis, a reference gas measurement and 10 sample measurements. Every ~10 samples we analysed a reference carbonate (in-house Carrara marble) for accuracy assessment and measured certified standards at the start and end of the measurement run (NBS-18, IAEA CO-1). For dolomite and ankerite an acid-reaction correction in accordance with Kim et al. (2015) was applied. Precision was determined via replicate analysis of reference materials and was about 0.05 ‰ for $\delta^{13}C$ and 0.05 ‰ for $\delta^{18}O$.

4. Petrography

4.1. Fine-grained calcite carbonatites (FGCC, samples DW002H, DW003, DW010)

These rocks are dominated by calcite (with occasional limonitised dolomite), with minor apatite, aegirine, biotite, quartz, baryte and rare fluorite. Dolomite-poor FGCC with magnetite, biotite and aegirine occur near the complex's margin, while dolomite-bearing, biotite- and clinopyroxene-free FGCC dominate the interior (Cooper, 1988). Porphyritic FGCC contains macrocrysts of magnetite, pyrochlore, apatite, tabular calcite and rhomboidal dolomite set in a granular calcite groundmass, randomly dispersed or flow-aligned along the margins of intrusive contacts (Fig. 2B & D) or cumulate-like zones in differentiated sheets of FGCC. In phenocryst-poor zones, the typically granular calcite groundmass may show spinifex-like textures of interlocking blades of dolomite and calcite (Cooper and Reid, 1991). The host FGCC surrounding the large xenolith itself *(DW002H)* exhibits banded flow textures (Figs. 2B-E) and contains calcite (~95%) with minor iron oxides/hydroxides and accessory pyrochlore (Fig. 3A) with no additional silicate minerals, except for accessory interstitial quartz (Fig. 5) at the immediate contact with the xenolith. Occasionally, the immediate contact between the xenolith and the FGCC exhibits ferroan dolomites exsolving hematite (DW002G, Fig. 2D), and a zone of baryte associated with tiny unidentified REE phases (<5 µm) at the immediate macroscopic contact.

4.2. Coarse-grained calcite carbonatites (CGCC, samples AFC213, DW005)

Besides calcite, coarse-grained calcite carbonatites (CGCC) comprise apatite, magnetite, clinopyroxene, pyrochlore, biotite and less abundant nepheline and K-feldspar. CGCC are texturally variable and may show flow banding comprising layers rich in magnetite and clinopyroxene and irregular segregations (schlieren) or pods of magnetite or pyrochlore (Cooper, 1988). While some CGCC are entirely composed of calcite (DW005; Fig. 3C), others host abundant magnetite, clinopyroxene and biotite aggregates (Fig. 3D). Clinopyroxene is euhedral and zoned (aegirine-augite cores to aegirine rims) and occasionally replaced by a pale blue amphibole (Cooper and Reid, 1998).

4.3. Ijolite-syenite suite (samples AFC093A, AFC267A, AFC268A, AFC269A, DW004)

Rocks of the ijolite-syenite suite display variable grain sizes and contain variable amounts of clinopyroxene, nepheline, calcite and orthoclase, with minor garnet, biotite, titanite and apatite, and occasional wollastonite, magnetite and zircon (Cooper, 1988). Thus, their composition ranges from urtite, ijolite and melteigite to nepheline syenite and syenite. Clinopyroxene is euhedral to subhedral, with inclusions of calcite and nepheline (Fig. 3F). Euhedral to strongly poikilitic nepheline is variably replaced by orthoclase (Figs. 3F-G). Nepheline in contact with calcite may form cancrinite in between (Cooper, 1988). Calcite and orthoclase occur as interstitial to poikilitic patches with the latter one often enclosing corroded remnants of nepheline. Small pools of calcite are situated between big pools of K-feldspar (Fig. 3E). Anhedral to subhedral dark andradite of variable size is associated with nepheline and clinopyroxene (Fig. 3F). Granular apatite occurs either evenly distributed or as clusters.

4.4. Nepheline silicocarbonatites (samples AFC093B-F, AFC267B-C, AFC268B, AFC269B-C)

These rocks are mineralogically transitional between those of the

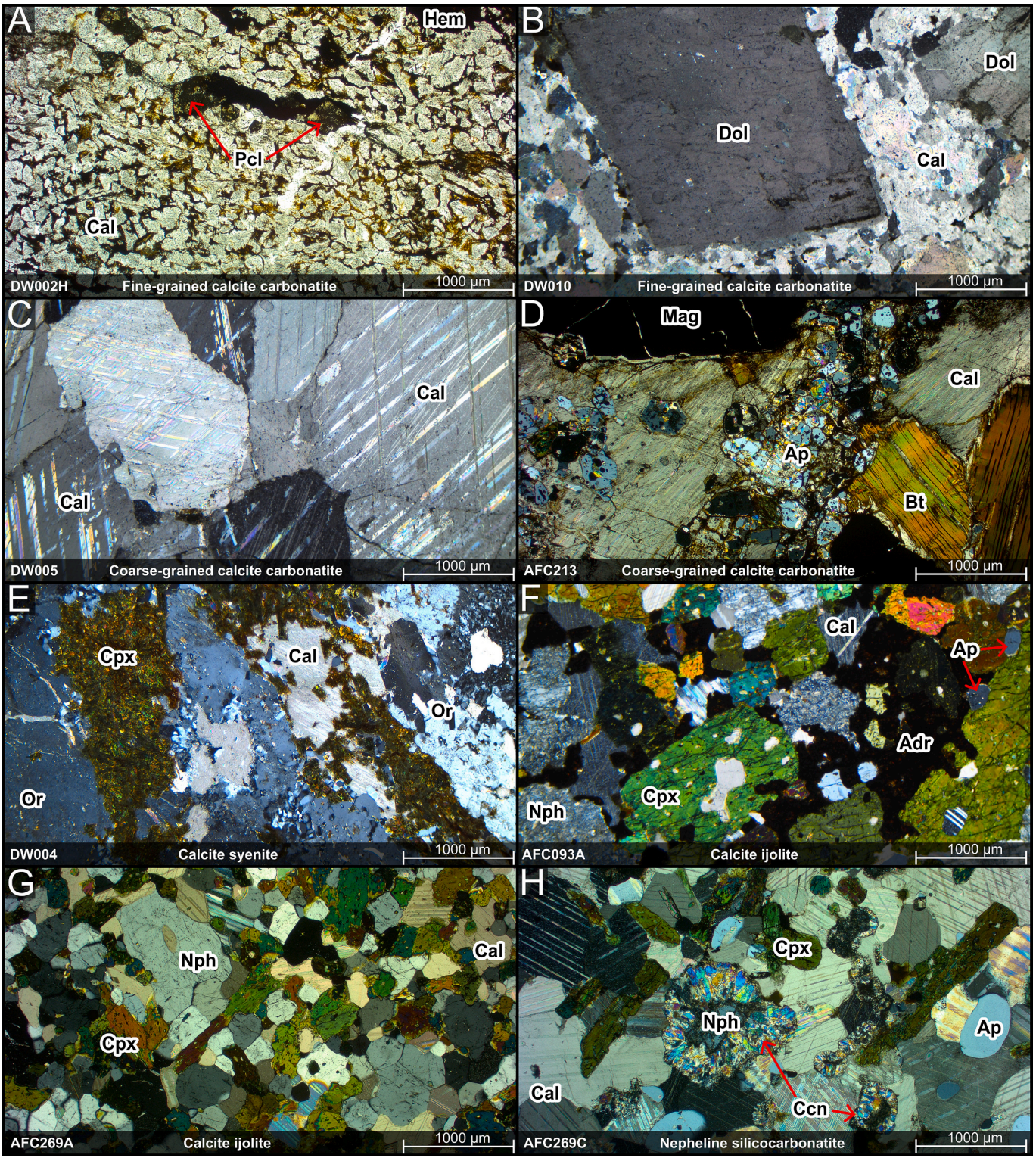

Fig. 3. Photomicrographs of the main lithologies of Dicker Willem (Namibia). A) Fine-grained calcite carbonatite (FGCC) with euhedral pyrochlore (euhedral) and secondary iron oxyhydroxides between calcite grains (DW002H). B) FGCC with rhomboidal dolomite macrocrysts (DW010). C) Coarse-grained calcite carbonatite (CGCC) entirely composed of calcite. D) CGCC with apatite, magnetite and biotite (AFC213). E) Syenitic sample composed of patchy orthoclase and altered polycrystalline clinopyroxene with interstitial calcite (DW004). F) Ijolite composed of clinopyroxene, altered nepheline, andradite and some calcite (AFC093A). G) Granular ijolite with clinopyroxene, nepheline and calcite (AFC269A). H) Nepheline silicocarbonatite with calcite, clinopyroxene, apatite and nepheline, with the latter being partly transformed to cancrinite (AFC269C).

ijolite-syenite suite and CGCC and have been previously termed nepheline sövites (Cooper and Reid, 1998). Fine to medium grained varieties can be texturally distinguished from coarser grained varieties often associated with ijolites They are dominated by calcite with significant amounts of nepheline, apatite, clinopyroxene, and andradite. The investigated samples show variable degrees of alteration expressed by replacement of nepheline by cancrinite (Figs. 3H), and the partial resorption of andradite and clinopyroxene, both of which being rich in calcite, nepheline or apatite inclusions.

4.5. Xenolith (samples DW002A-002F)

Previous studies distinguished three types of xenoliths at Dicker Willem, namely xenoliths of the ijolite-syenite series, of the nepheline silicocarbonatites and CGCC xenoliths within the FGCC (Figs. 1 & 2C, E; Cooper and Reid, 1998). The studied large xenolith (Figs. 2C-D), in contrast, represents a transitional variety that combines mineralogical features of all three xenolith types (see discussion). The xenolith exhibits an irregular shape with a diameter of about 5 to 9 m. A blurred semi-systematic zonation without clear boundaries emerges from the centre of the xenolith towards its margin. This zonation reflects areas of different mineralogical development and a progressive deviation of the modal mineralogy. A steadily increasing calcite content until the composition strongly resembles that of the surrounding FGCC can be observed (Fig. 5).

The central part (samples DW002A & 002B) consists of clinopyroxene (30–50%), orthoclase (8–48%), nepheline (4–29%), and calcite (8–25%), with minor apatite and andradite (Fig. 5). Clinopyroxene is commonly euhedral (Fig. 4A-B) but also occurs as accumulations of smaller and mostly anhedral crystals with tiny inclusions of calcite, albite and ancylite-(Ce) some of which are partly overgrown by blue arfvedsonite (Fig. 4C). Orthoclase occurs as tabular crystals, but is more commonly found as larger sub- to anhedral masses (Figs. 4A & D), euhedral-anhedral nepheline is partly replaced by orthoclase (Figs. 4B & 6A). Calcite is interstitial to clinopyroxene, orthoclase and nepheline (Figs. 4A-D). Very small strontianite can be found as inclusions in calcite. Apatite appears as evenly distributed and euhedral crystals (~0.5 mm), partly as granular clusters. Andradite is oscillatory zoned and poikilitic with inclusions of heavily altered nepheline and minor clinopyroxene (Fig. 3A).

In the intermediate part (samples DW002C & 002D), calcite increases in abundance, reaching up to 70%, the most abundant silicate minerals are clinopyroxene (up to 50%) and orthoclase (up to 40%), nepheline and apatite are rare, andradite is lacking (Fig. 5). Orthoclase contains inclusions of clinopyroxene and relics of nepheline (Figs. 4E-F), gradually decreases in abundance down to 5% outwards the xenolith, and texturally progresses towards subhedral or partially resorbed grains (Fig. 4F). Occasionally, biotite and interstitial quartz are present (Fig. 4E).

The outer parts of the xenolith (samples DW002E & 002F) are dominated by coarse calcite (up to 96%) that occurs as granular patches. Clinopyroxene, apatite, corroded relics of orthoclase and interstitial quartz are rare, nepheline is absent (Fig. 4G-H). Instead, euhedral biotite (up to 5 mm in size) constitutes up to 12% of the rock, often associated with secondary hematite (up to 5%), altered clinopyroxene and relictic orthoclase (Fig. 6B). Some orthoclase appears as inclusions in biotite (Fig. 6C), while others show marginal replacement by biotite (Fig. 6B). Furthermore, biotite contains inclusions of apatite as well. Occasionally, rutile has been detected next to fragmented clinopyroxene. Accessory pyrochlore appears as euhedral crystals about 0.7 mm in size.

The textural and mineralogical changes observed in the investigated xenolith are summarised in Figs. 5, 7 & 11. From the inner part to the margin of the xenolith, the rock names would change from calcite ijolite (sample DW002A) and calcite nepheline syenite (DW002B) in the inner part, via calcite syenite (sample DW002C), and clinopyroxene silicocarbonatite (DW002D) to coarse-grained calcite carbonatite in the marginal area DW002E-002F.

5. Whole rock data

Whole-rock data for the different zones of the investigated xenolith and the host FGCC (Table 2) cover the range of previously published data for calcite carbonatites, nepheline silicocarbonatites, and ijolites (Fig. 8; Cooper and Reid, 1998, Ogungbuyi, 2020). Central samples (DW002A and 002B) fall in the ijolite field, intermediate samples (DW002C and 002D) into the nepheline silicocarbonatite field, all other samples fall in the calcite carbonatite field, indicating a continuous process rather than two different rock suites (Figs. 8A-C).

All samples exhibit the LREE-enriched primitive mantle-normalised pattern, with intermediate and marginal samples showing stronger LREE enrichments than ijolites (Fig. 8D). The marginal samples (DW002E and 002F) show the highest REE, Sr and Nb contents (Fig. 8D; Table 2), in line with the occurrence of accessory strontianite, pyrochlore, and REE phases in these samples, while Ba has its highest contents around the central xenolith.

In contrast, a significant depletion of Fe, Na, K, Si, and some P is evident with increasing proximity to the contact (Figs. 8A-C, Table 2). Please note that all xenolith samples show carbonatitic tendencies according to the discrimination diagram of Samoilov (1991, Fig. 8E). The $\delta^{13}C_{VPDB}$ and $\delta^{18}O_{VSMOV}$ values (Table 3) are in accordance with previous data (Reid and Cooper, 1992), following a linear trend from the primary igneous carbonatite (PIC) box (Taylor et al., 1967) for the central samples towards higher $\delta^{13}C_{VPDB}$ and $\delta^{18}O_{VSMOV}$ values for the marginal sample and the host FGCC (Fig. 8F).

6. Mineral compositions

The mineralogical composition of the xenolith exhibits a notable evolution in clinopyroxene from aegirine-augite ($Ca_{0.8}Na_{0.2}Fe_{0.6}Mg_{0.4}Si_2O_6$) at its core to aegirine ($Na_{0.8}Ca_{0.2}Fe_{0.8}Mg_{0.2}Si_2O_6$) near the contact zone, consistent with previously published data (Cooper and Reid, 1998; Table 4; Fig. 9A). Moving from the central to the intermediate zone, there is a subtle shift in composition, with one measurement indicating an augitic composition, while the majority of analyses falls within the lower aegirine-augite field. Sample DW002E displays a significant deviation, showing a continuous evolution from aegirine-augite to intermediate compositions and endmember aegirines.

The mica in the xenolith is identified as biotite (EDX), with an average X_{Mg} of 0.51, which is characteristic of silicate rocks, but distinct from mica found in other carbonatites (Fig. 9B). Similarly, the mica in one studied CGCC sample is also biotite, with an average X_{Mg} of 0.60, comparable to the mica within the xenolith. It is important to note that the mica compositions are derived from semi-quantitative analysis using μXRF, which carries a larger margin of error. However, the data is considered a reliable estimate and is not expected to differ significantly from the EPMA data, based on comparisons made with the clinopyroxene data. The detailed analyses can be found in Supplementary File 1.

7. Discussion

Systematic variations in mineral abundances, mineral compositions, textures and whole rock geochemistry in the investigated xenolith indicate variable degrees of interaction between precursor ijolite and carbonatitic magma and/or carbohydrothermal fluids. These interactions not only account for the formation of silicocarbonatite but also carry broader implications for similar systems, as further explored in the following.

7.1. Reinterpreting the origin of the ijolite-syenite suite at Dicker Willem

Rocks of the so-called ijolite-syenite suite at Dicker Willem represent <0.2% of the exposed carbonatites and have been previously interpreted

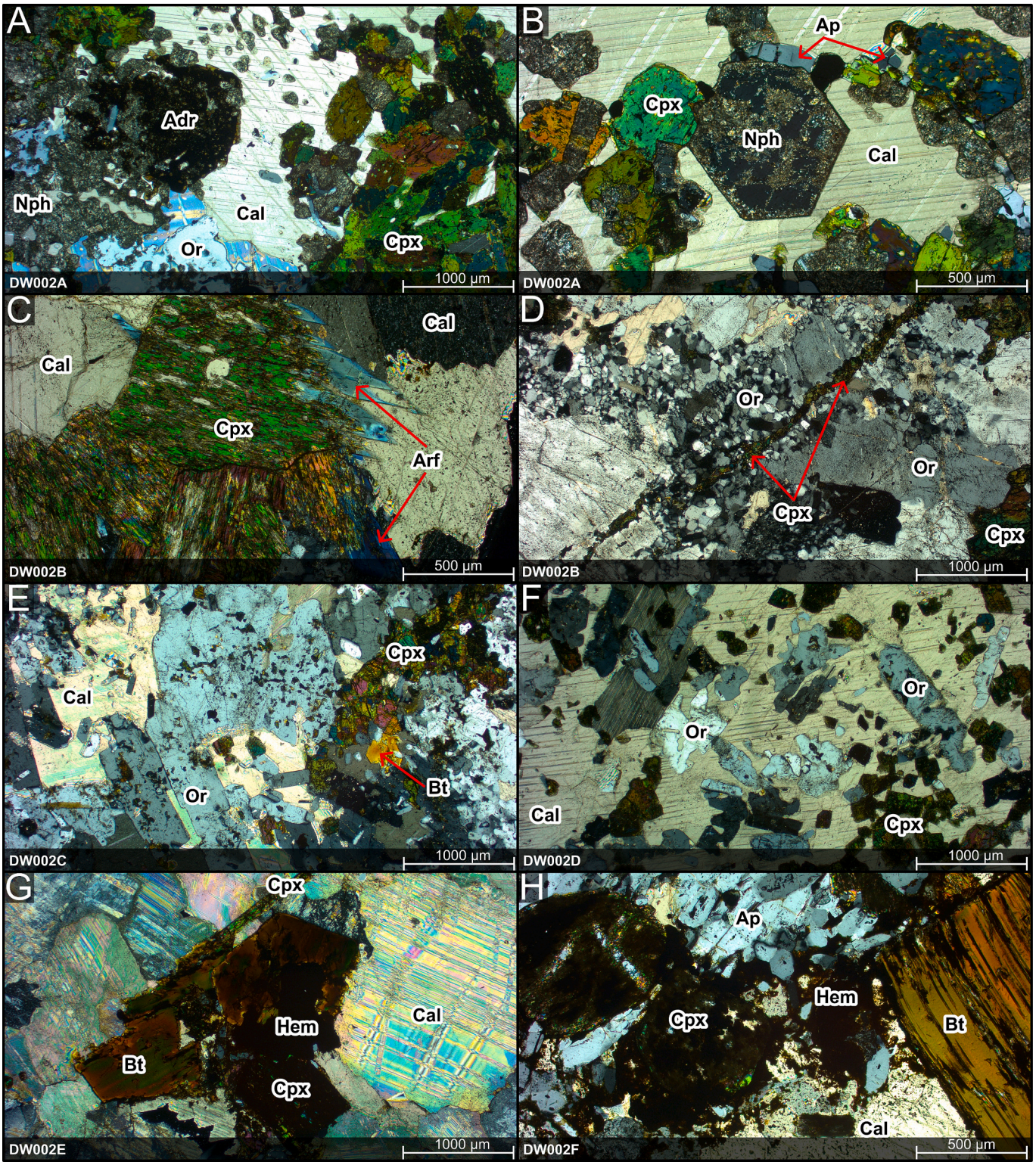

Fig. 4. Photomicrographs of the investigated xenolith. A) Euhedral andradite, with an assemblage of clinopyroxene, nepheline and orthoclase in a calcite matrix in central xenolith sample (DW002A). B) Euhedral and partially altered nepheline crystal with other more extensively altered nephelines (intergrown with clinopyroxenes) embedded in calcite groundmass (DW002A). C) Clinopyroxene being partly replaced by arfvedsonite (DW002B). D) Subhedral and granular orthoclase with euhedral and vein-like clinopyroxene (DW002B). E) Tabular orthoclase surrounded by calcite with clinopyroxene inclusions. Small biotite occurs near clinopyroxene. (DW002C). F) Partially resorbed tabular orthoclase in poikilitic calcite (DW002D). G) Calcite with biotite (intergrown with hematite) and altered clinopyroxene (DW002E). H) Euhedral biotite and a cluster of apatite next to altered clinopyroxene with hematite (DW002F).

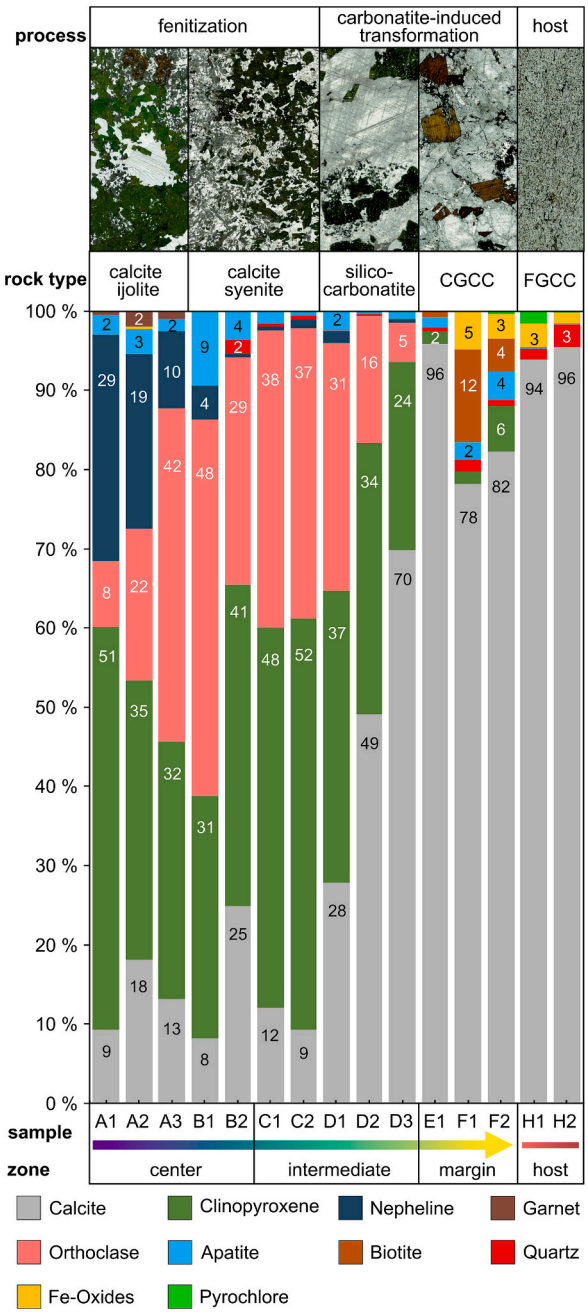

Fig. 5. The modal mineral content of the samples taken in the xenolith profile (Fig. 2D). Rock type variations (according to the classification scheme of Le Maitre et al., 2002) induced by fluid (fenitization) and magma (carbonatite-induced) overprinting are assigned. Scans of the corresponding thin sections from A-D showing the change in mineralogy and texture. (For interpretation of the references to colour in this figure legend, the reader is referred to the web version of this article.)

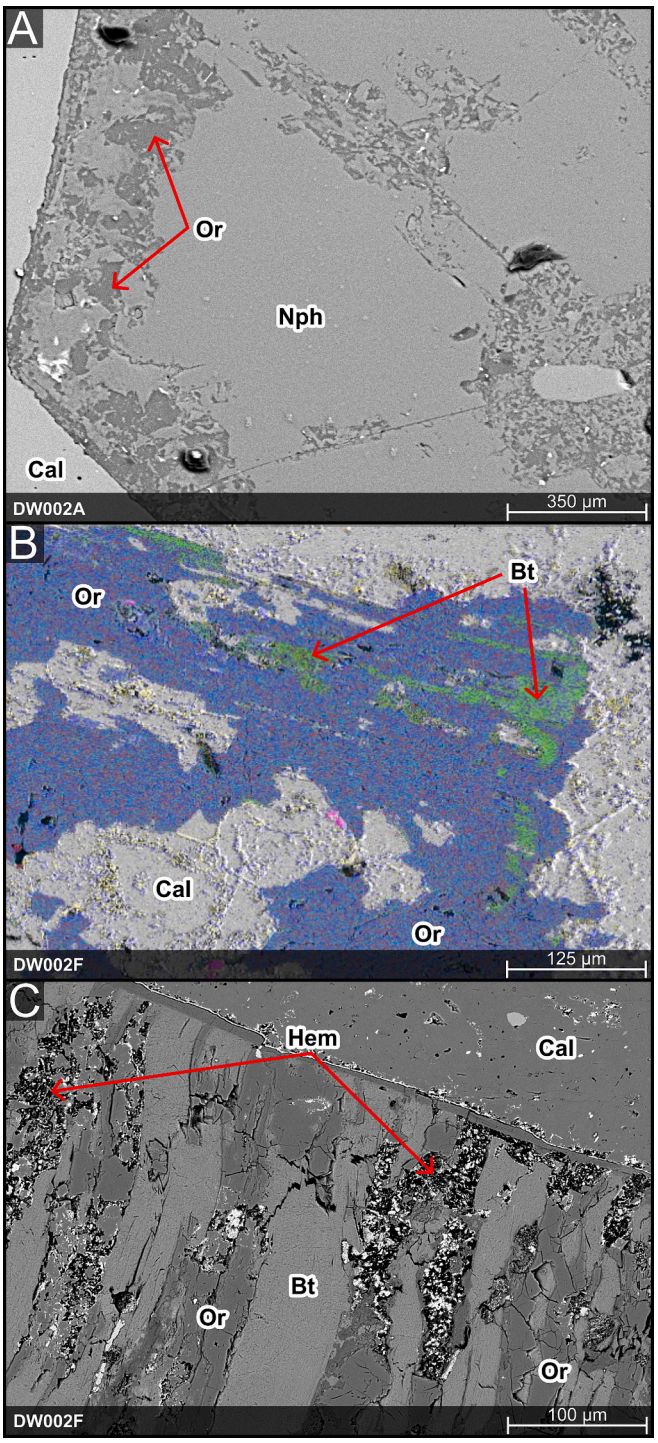

Fig. 6. A) BSE-image of euhedral nepheline (Fig. 4B) showing the beginning replacement of nepheline by orthoclase. B) EDX-map of a heavily resorbed orthoclase and partial replacement by biotite in the outer xenolith zone (DW002F). C) Biotite intergrown with orthoclase in medium sized calcite (DW002F). Orthoclase is partially replaced by hematite.

to represent rare remnants of cumulate rocks that formed from a parental nepheline silicocarbonatite (nepheline sövite) magma, later disrupted by intrusion of first CGCC, later by FGCC (Cooper, 1988; Cooper and Reid, 1998). The ijolites-syenites, silicocarbonatites (nepheline sövite) and both carbonatite varieties exhibit remarkably similar Nd, Sr and Pb-isotopic compositions, reinforcing the idea of a common origin (Ogungbuyi, 2020; Reid and Cooper, 1998). Furthermore, based on overlapping carbon and oxygen isotope ratios of calcite in CGCC and ijolite (Fig. 8F), Reid and Cooper (1992) concluded that both rocks are the products of two coexisting immiscible melt fractions and, hence, share the same origin. The close correspondence of clinopyroxene and nepheline compositions in the CGCC and ijolites further supports this contention.

Field relationships and the co-crystallization of clinopyroxene, nepheline, and calcite indicate that calcite-bearing ijolite represents cumulate assemblages rather than a parental magma (Cooper and Reid, 1998). Thus, Cooper and Reid (1998) proposed that the hypothetical

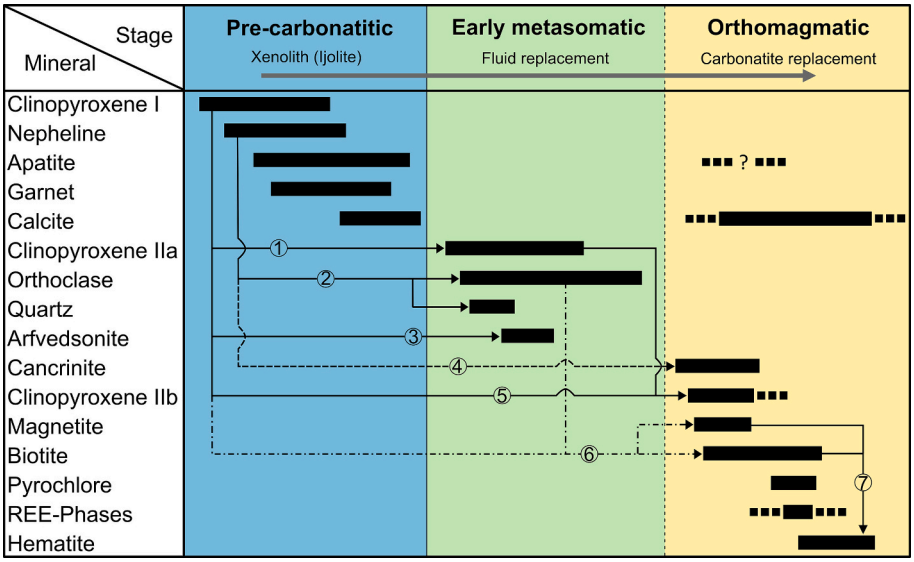

Fig. 7. Paragenetic scheme of the xenolith's mineralogy. The pre-carbonatitic stage represents the initial ijolitic paragenesis, the early metasomatic stage reflects a transitional stage during the carbohydrothermal overprint of the ijolitic mineral assemblage (fenitization) and the orthomagmatic stage the recrystallization and mineralization of new minerals during the magmatic replacement (carbonatization). Arrows indicate the source for components of minerals formed during the different stages: 1) Recrystallization of clinopyroxene 2) Replacement of nepheline by orthoclase and quartz 3) Replacement of nepheline by cancrinite 4) Replacement of clinopyroxene by arfvedsonite 5) secondary (re-)crystallization of clinopyroxene 6) Formation of biotite by (partial) dissolution of clinopyroxene and K-feldspar and formation of magnetite by excess iron. 7) Oxidation of magnetite and exsolved hematite from biotite.

parental magma was a nepheline silicocarbonatitic melt, as represented by nepheline silicocarbonatite pockets present in the CGCC. Ogungbuyi (2020) found limited evidence for the formation of carbonatites at Dicker Willem from parental hybrid carbonate-silicate magmas. The data instead supports their direct origin from very low-degree mantle melts.

Recent models emphasize the possibility of a metasomatic formation of ijolitic rocks by interaction of carbonatite magma with silicate wall rocks leading to consumption of Ca and Mg from the carbonatite magma and passive enrichment of Na in the residual melt, facilitating the assimilation of Si and Al and lowering the solidus generating an alkaline silicate magma ultimately leading to ijolite formation (Anenburg and Walters, 2024; Vasyukova and Williams-Jones, 2022). This was previously suggested for ijolites from the Livaara Complex (Finland), envisioned to have formed by partial melting of high-grade fenitized country-rock (Kramm, 1994). Applying such a mechanism, calcite ijolites at Dicker Willem rather represent interaction products between carbonatitic magma with siliceous basement rocks, similar as proposed e.g., for Kovdor and Palabora (Gudelius et al., 2023; Vasyukova and Williams-Jones, 2022).

Applying such models would also resolve the controversy surrounding the potential existence of a silicocarbonatitic parental melt, particularly regarding silica content. At crustal pressures and temperatures below 1000 °C, silica levels in carbonatite melts are typically below 2% (often <1%), particularly when saturated with silicate minerals or an immiscible silicate liquid (Anenburg and Aslam, 2024; Brooker and Kjarsgaard, 2011; Martin et al., 2013). While alkali-poor carbonatite melts ($Na_2O + K_2O < 10\%$) may contain slightly higher SiO_2, it rarely exceeds 10% (Brooker and Kjarsgaard, 2011; Nabyl et al., 2020; Otto and Wyllie, 1993). Yet, an unrealistic ~20% SiO_2 would be required to enable the formation of characteristic silicocarbonatite-hosted minerals, far exceeding experimental observations (Zhu et al., 2025).

7.2. Metasomatic replacement of ijolite: Fenitization by carbonatite-derived fluids

In the central part of the xenolith, euhedral nepheline shows incipient replacement by orthoclase (Figs. 4B & 6A). In the medial parts, replacement is more intense and results in the complete disappearance of nepheline. Orthoclase textures change from anhedral replacement patches and granular textures in the central part (Figs. 4A & D) to tabular euhedral in the intermediate areas (Fig. 4E), while in the marginal calcite-rich areas, orthoclase dissolves again, leaving only relicts (Fig. 6B). This process is mirrored by the changing modal abundances of nepheline and orthoclase: While in the central parts of the xenolith (samples DW002A1 to DW002B1), the abundance of orthoclase clearly anti-correlates with nepheline, the modal abundance of orthoclase decreases again from sample DW002B2 (where nepheline is already virtually absent) until it completely disappears in sample DW002E1 (Fig. 10). Correspondingly clinopyroxene compositions evolve from augite to aegirine-augite (sample DW002A-D; Fig. 9A).

These observed modifications of the xenolith (especially in its inner parts) are commonly found in potassic fenite aureoles surrounding carbonatites (Elliott et al., 2018; Le Bas, 2008), where metasomatic reactions of synmagmatic carbohydrothermal fluids and felsic host rocks form high amounts of orthoclase, albite, Na-bearing clinopyroxene and amphibole (Kresten and Morogan, 1986). Such carbonatite-derived fluids are compositionally diverse but typically highly oxidizing, aqueous-dominated, and range in temperature from 500 to 700 °C (e.g., Williams-Jones and Palmer, 2002). The formation of Na-amphibole (Fig. 4C) and the instability of nepheline under hydrous conditions (Kim and Burley, 1971) point to the presence of an aqueous fluid causing an initial modification of the original ijolitic composition. Large amounts of CO_2 in the fluid phase will promote orthoclase formation at temperatures of up to 600 °C (Rubie and Gunter, 1983). Given that the Dicker Willem complex represents a subvolcanic intrusion (Cooper, 1988), a pressure range of approximately 1–3 kbar is considered reasonable for this process. The oxygen fugacity was likely high, as evidenced by Fe^{3+}-bearing andradite or evolving aegirine component, within the xenolith (Figs. 4A & 9A).

Under magmatic conditions in carbonatitic systems (1000 °C, crustal pressures) silica activities are too low to permit crystallization of minerals like orthoclase, quartz, or orthopyroxene (Anenburg and Guzmics, 2023; Barker, 2001). Under such conditions, phlogopite typically forms, as seen in natural “black walls” at silicate-carbonatite contacts (Chmyz

Table 2
Whole rock analysis (XRF, ICP-MS) of the xenolith samples plus directly surrounding host rock (FGCC), and selected samples of close by DW lithologies.

Sample no.	DW002A	DW002B	DW002C	DW002D	DW002E	DW002F	DW002H1	DW002H2	DW004	DW003	DW010	DW005
Rock type	(Xenolith)	(Xenolith)	(Xenolith)	(Xenolith)	(Xenolith)	(Xenolith)	(Host rock)	(Host rock)	(Syenite)	(FGCC)	(FGCC)	(CGCC)
Na_2O (%)	2.97	2.85	2.04	1.57	0.26	0.07	0.00	0.06	2.21	0.01	0.27	0.18
MgO (%)	2.64	2.66	2.32	1.45	0.69	0.65	0.18	0.21	0.80	0.09	11.62	0.32
Al_2O_3 (%)	9.64	5.91	1.20	1.40	0.37	0.66	0.07	0.09	8.58	0.39	0.00	0.31
SiO_2 (%)	39.11	42.66	21.56	17.47	3.58	3.64	2.20	1.84	41.99	1.61	0.14	2.78
P_2O_5 (%)	1.08	2.81	1.17	0.58	0.89	0.58	0.03	0.07	1.06	0.28	7.96	0.58
K_2O (%)	3.60	4.35	0.89	1.11	0.28	0.40	0.03	0.04	7.20	0.29	0.01	0.15
CaO (%)	19.75	19.55	35.14	39.08	47.37	46.08	48.77	47.88	16.18	49.60	34.22	48.72
TiO_2 (%)	0.14	0.12	0.12	0.07	0.10	0.17	0.05	0.07	0.11	0.01	0.09	0.04
MnO (%)	0.47	0.51	0.48	0.36	0.23	0.39	0.41	0.45	0.21	0.11	0.84	0.19
Fe_2O_3 (%)	9.08	9.74	8.09	5.36	2.48	5.08	1.76	2.21	8.06	0.35	2.80	1.16
LOI (%)	10.67	8.10	23.93	29.07	38.77	38.39	41.34	40.74	12.02	41.24	33.76	54.44
Total	99.15	99.27	96.94	97.51	95.02	96.11	94.84	93.67	98.40	93.97	91.70	94.54
Trace elements (ppm)												
Li	5.9	8.3	24.4	8.2	12	19	2.6	6.9	9.2	0.8	4.9	3.0
Be	9.3	14	17	8.1	3.4	3.8	3.4	4.4	14	0.5	34	1.2
Sc	3.0	5.1	2.4	1.4	1.7	3.0	2.0	4.5	5.0	0.4	37	0.6
V	291	341	370	182	95	115	84	117	469	8.2	193	35
Cr	3.2	4.1	1.2	0.4	1.1	1.1	0.4	0.9	1.6	0.9	0.3	3.2
Co	3.6	3.2	2.8	1.8	2.9	8.1	0.5	1.0	2.7	0.4	0.8	1.2
Ni	0.9	1.0	0.6	0.3	1.1	3.1	0.3	0.6	1.0	0.3	0.1	1.0
Cu	2.1	1.6	1.7	2.4	3.8	6.2	1.5	3.3	2.7	3.6	1.4	2.7
Zn	175	178	152	90	47	98	35	55	139	3.7	613	17
Rb	68	85	12	18	15	21	0.6	0.8	119	5.7	0.1	4.2
Sr	1831	1541	3407	4558	6346	4053	2738	2519	1153	7095	6868	7743
Y	40	47	54	38	59	67	80	84	29	44	400	43
Zr	157	303	262	105	57	26	33	64	246	5.1	94	39
Nb	24	112	132	26	269	179	1102	2799	95	23	247	82
Mo	0.5	0.3	5.2	0.7	6.1	31	10	9.1	13	1.4	8.1	0.9
Sb	0.0	0.1	0.2	0.1	0.3	0.5	0.3	0.5	0.6	0.1	2.1	0.0
Cs	0.5	0.2	0.1	0.0	0.2	0.2	0.1	0.0	0.2	0.0	0.0	0.1
Ba	614	1108	1174	625	706	489	1139	1853	1207	491	12,232	844
Hf	2.5	5.5	4.2	2.5	0.5	0.4	0.7	1.1	4.2	0.1	1.6	0.5
Ta	1.4	3.0	1.9	0.5	5.8	3.7	0.8	2.2	0.7	0.9	0.2	1.9
W	3.0	2.5	2.3	1.3	2.9	1.7	1.2	1.1	2.3	0.4	12	0.8
Pb	3.3	4.4	3.6	3.8	6.7	11	4.4	8.2	7.8	3.2	62	3.9
Bi	0.0	0.0	0.0	0.0	0.0	0.0	0.1	0.1	0.0	0.0	0.3	0.0
Th	28	35	23	15	14	17	34	52	13	6.7	186	8.7
U	3.6	6.3	3.5	3.0	7.7	18	4.9	7.6	11	3.3	0.9	7.2
REE												
La	91	122	142	157	214	218	622	550	108	191	754	199
Ce	222	310	325	342	457	471	1413	1260	248	401	1840	422
Pr	27	39	39	39	52	53	169	151	30	44	240	48
Nd	107	153	150	144	187	191	655	588	114	158	1013	175
Sm	20	27	26	23	30	33	105	98	18	25	195	26
Eu	5.7	7.2	7.4	5.9	8.3	9.1	27	26	4.6	6.8	62	6.7
Gd	15	18	19	15	22	24	60	59	11	17	159	17
Tb	1.9	2.3	2.6	1.7	2.7	3.1	5.9	6.1	1.3	2.1	22	2.0
Dy	9.5	11	13	7.9	13	15	23	24	6.2	10	101	9.1
Ho	1.6	1.8	2.1	1.3	2.2	2.5	3.3	3.4	1.0	1.6	16	1.5
Er	3.9	4.1	4.6	3.1	4.9	5.6	7.1	7.3	2.5	3.8	35	3.5
Tm	0.5	0.5	0.6	0.4	0.6	0.7	0.8	0.9	0.3	0.5	4.0	0.4
Yb	3.1	3.2	3.1	2.6	3.2	4.0	4.4	4.8	2.3	2.7	22	2.5
Lu	0.5	0.5	0.5	0.4	0.4	0.6	0.6	0.6	0.4	0.4	2.9	0.4
TREE	509	699	735	743	996	1029	3096	2780	548	863	4466	913

et al., 2025; Viladkar, 2015). Modelled phase diagrams further indicate that K-feldspar does not form at magmatic temperatures in these systems (Anenburg and Walters, 2024). Thus, the initial metasomatic replacement of nepheline is best described to have occurred by an aqueous Na-bearing, K-rich and CO_2-bearing carbohydrothermal fluid, reflecting its carbonatitic origin.

Abundant orthoclase together with clinopyroxene corresponds to a rock with syenitic composition although the process modifying it is metasomatic in nature. Thus, in the case of Dicker Willem, intense pervasive feldspatization of calcite ijolites leads to the formation of non-magmatic calcite-rich syenitic rocks (e.g., sample DW004; Cooper and Reid, 1998), and this process, rather than magmatic differentiation, explains the compositional variation in the ijolite-syenite suite of Cooper (1988). While the exact role of carbohydrothermal fluids and their composition remains speculative, the replacement of nepheline by orthoclase is envisioned to occur either through the interaction with Na-bearing and K-rich fenitizing carbohydrothermal fluids (1A, 1C, and 1D) or by utilizing the K inherent within the nepheline itself (1B).

$$\text{nepheline} + \text{K} - \text{bearing fluid} \rightarrow \text{orthoclase} + \text{residual fluid}$$

$$3\,Na_3K(Al_4Si_4O_{16}) + K^+ + 16\,H_2O \rightarrow 4\,KAlSi_3O_8 + 9\,Na^+ + 8\,Al(OH)_4^- \quad (1A)$$

$$\text{nepheline} + \text{K} - \text{poor fluid} \rightarrow \text{orthoclase} + \text{quartz} + \text{residual fluid}$$

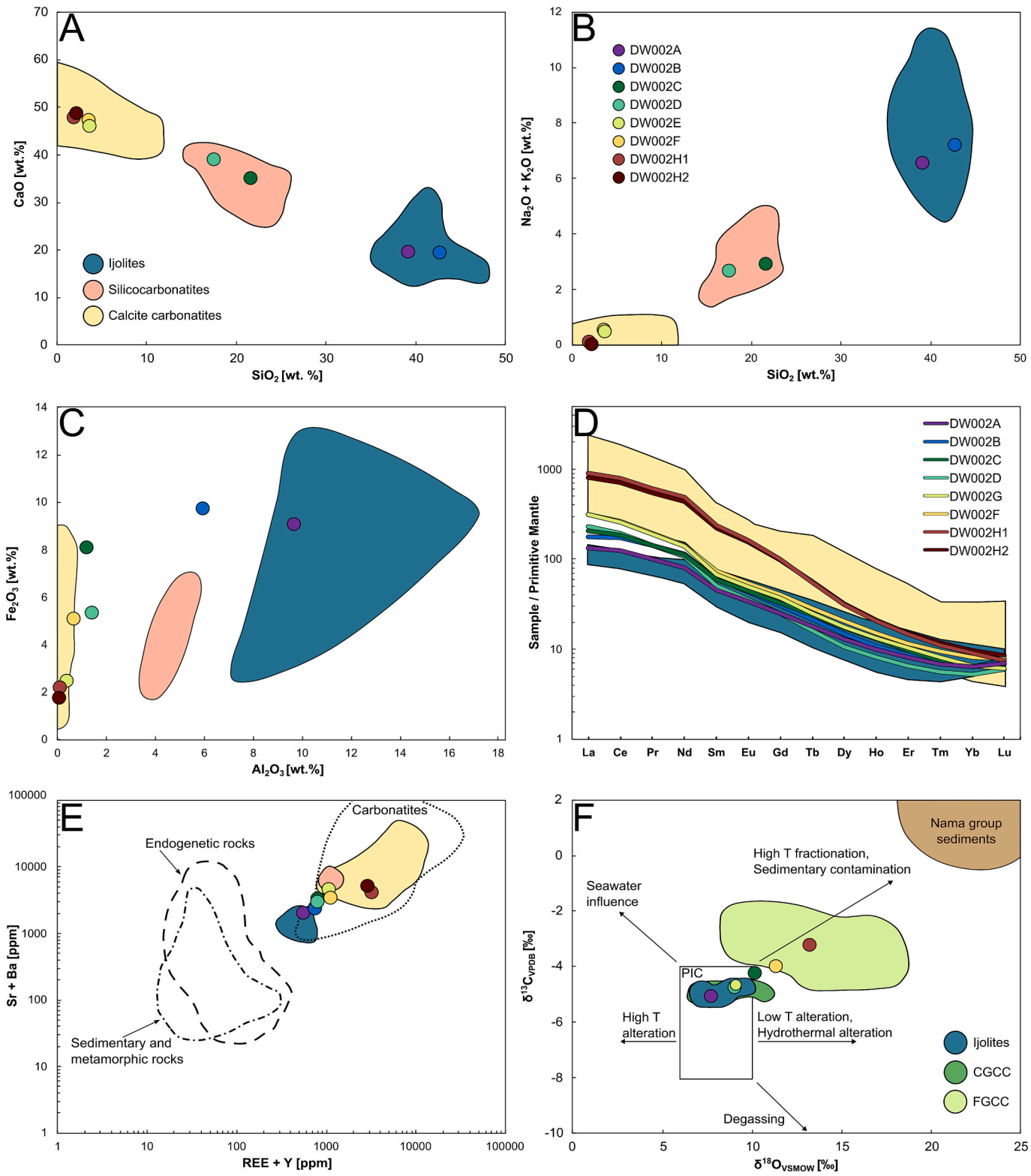

Fig. 8. Whole-rock geochemical and stable isotope (C and O) data for the investigated xenolith compared to previous data for ijolites, silicocarbonatites, and carbonatites of the Dicker Willem Complex from Cooper and Reid (1998) and Ogungbuyi (2020). A)-B) Binary (Harker) diagrams of SiO_2 versus CaO and the total alkali content, respectively. The main lithologies (literature data) of Dicker Willem are shown for comparison. C) Binary Al_2O_3 vs $Fe_2O_{3,Total}$ diagram. D) Primitive mantle normalised REE pattern of the xenolith samples. Fields for calcite carbonatite and ijolite are shown for comparison. E) Discrimination diagram of carbonatites based on Sr + Ba vs REE + Y after Samoilov (1991). F) Carbon and oxygen isotope ratios (relative to VPDB and VSMOW) of investigated profile samples, main lithologies of Dicker Willem (Reid and Cooper, 1992) and regional Nama group sediments (Ries et al., 2009). Field of primary igneous carbonatite (PIC) after Taylor et al. (1967).

Table 3
Bulk-rock carbonate C and O isotope composition of the investigated Dicker Willem xenolith.

Sample	$\delta^{13}C_{VPDB}$ [‰]	SD	$\delta^{18}O_{VPDB}$ [‰]	SD	$\delta^{18}O_{SMOW}$ [‰] (calculated)
DW002A	−5.09	0.18	−22.51	0.18	7.71
DW002C	−4.28	0.06	−20.13	0.05	10.16
DW002D	−4.78	0.05	−21.23	0.06	9.04
DW002E	−4.02	0.04	−18.98	0.05	11.35
DW002F	−4.73	0.04	−21.19	0.03	9.08
DW002H	−3.25	0.04	−17.19	0.04	13.20

$$Na_3K(Al_4Si_4O_{16}) + 4\,H_2O \rightarrow KAlSi_3O_8 + SiO_2 + 3\,Na^+ + 3\,Al(OH)_4^- \quad (1B)$$

nepheline + K − bearing fluid → orthoclase + residual fluid

$$3\,NaAlSiO_4 + K^+ + 4\,H_2O \rightarrow KAlSi_3O_8 + 3\,Na^+ + 2\,Al(OH)_4^- \quad (1C)$$

nepheline + K − bearing fluid → orthoclase + residual fluid

$$NaAlSiO_4 + K^+ + 2\,SiO_2 \rightarrow KAlSi_3O_8 + Na^+ \quad (1D)$$

In the first three reactions, Na and Al are released and can subsequently be incorporated into the recrystallization process of augite to form aegirine-augite and contribute to the formation of mica (see chapter 7.3). Rubie and Gunter (1983) proposed that potassium preferentially enters feldspar, while sodium migrates into the fluid at temperatures below 450 °C. This shift causes coexisting pyroxenes to become increasingly Na-bearing, a pattern that aligns well with our measured clinopyroxene compositions (Fig. 9A). A critical factor in these transformations is the availability of K, which directly influences the extent of orthoclase formation. Mass balance calculation assessing the compositional and volume changes with respect to the replacement of nepheline by orthoclase, indicates that K must be introduced to the system. Assuming an original orthoclase-free composition with 40 modal% nepheline (sample AFC093F) transforming to a nepheline-free syenitic composition with 60 modal% orthoclase (sample DW004), the introduction of 13.5 wt% K is indicated (calculated after the method of Gresens, 1967). Compared to reaction 1A, the interaction with a K-deficient carbohydrothermal fluid (as in reaction 1B) results in reduced orthoclase formation and the release of silica. Similarly, in fenites alkalis are exchanged for silica, which is then mobilised and later precipitated as quartz (e.g. Sokli, Finland; Vartiainen and Woolley, 1976). Accordingly, in samples where nepheline is almost entirely replaced by orthoclase (e.g. DW002B), accessory late-stage quartz is observed. The quartz could have formed from post-magmatic silicification, but interestingly there is no quartz in samples where there are still remnants of nepheline. Any excess silica (SiO_2) produced could further react with the fenitizing fluid, leading to additional transformations of any remaining nepheline, as illustrated in reaction 1D.

7.3. Ijolite transformation through interaction with carbonatite magma

Within the xenolith towards the interface with the host rock, clinopyroxene is rare (Fig. 5), always euhedral if not partially resorbed (Figs. 4G-H) and aegirine-rich (Fig. 9A). Biotite starts to crystallize around clinopyroxene (DW002C; Fig. 4E) and becomes the major silicate mineral closer towards the interface forming euhedral crystals but also replacing resorbed remains of orthoclase (DW002E and F; Figs. 6B-C & 11). Together with these minor magnetite (later oxidised to hematite), accessory quartz and pyrochlore are present. This is interpreted to result from direct interaction with carbonatite magma. Coinciding with the resorption of primary augite and orthoclase, it is reasonable to assume that the related release of K, Si, Al and Fe favours biotite + magnetite formation, according to the following schematic reaction (2):

orthoclase + aegirine − augite + carbonatite melt → biotite + aegirine + magnetite + calcite + silica (2)

$$KAlSi_3O_8 + 2(Ca_{0.5}Na_{0.5})(Fe^{3+}{}_{0.5}Mg_{0.25}Fe^{2+}{}_{0.25})[Si_2O_6] + Mg^{2+} + 4\,Fe^{2+} + 2\,H_2O + CO_3{}^{2-} + 4\,O_2 \rightarrow KMg_{1.5}Fe^{2+}{}_{1.5}Si_3AlO_{10}(OH)_2 + NaFe^{3+}Si_2O_6 + Fe^{2+}Fe^{3+}{}_2O_4 + CaCO_3 + 2\,SiO_4{}^{4-} + 2H^+$$

Table 4
Representative major-element compositions of clinopyroxene from within the studied xenolith.

Sample	DW002A	DW002A	DW002D	DW002D	DW002E	DW002E	DW002F	DW002F
Mineral	Augite	Augite	Aeg-Aug	Aeg-Aug	Aeg-Aug	Aegirine	Aegirine	Aegirine
SiO_2	50.44	51.07	51.98	51.98	52.35	52.33	51.89	51.87
TiO_2	0.35	0.34	0.41	0.38	0.47	0.41	1.93	0.50
ZrO_2	b.d.	b.d.	0.10	0.10	0.30	0.33	0.31	0.12
Al_2O_3	1.19	1.05	0.81	0.68	0.31	0.37	0.23	0.12
Cr_2O_3	b.d.	b.d.	b.d.	b.d.	b.d.	0.04	b.d.	b.d.
FeO^T	16.82	17.00	17.72	18.35	22.48	26.01	28.62	28.62
MnO	0.97	1.02	0.92	0.98	0.09	0.00	0.00	0.00
MgO	7.36	7.06	6.74	6.26	4.36	2.38	0.23	0.67
CaO	19.89	18.17	15.05	13.82	7.20	3.40	0.07	1.11
Na_2O	2.27	3.27	5.16	5.74	9.31	11.35	12.71	12.53
K_2O	0.00	0.00	0.00	0.05	0.06	0.00	0.01	0.00
$Total_{calc}$	100.00	99.84	100.15	99.72	99.13	99.30	98.70	98.52
Formula based on 4 cations and 6 oxygens								
Si^{4+}	1.946	1.965	1.979	1.987	2.005	2.008	2.019	2.017
Ti^{4+}	0.010	0.010	0.012	0.011	0.013	0.012	0.056	0.015
Zr^{4+}	0.000	0.000	0.002	0.002	0.006	0.006	0.006	0.002
Al^{3+}	0.054	0.048	0.036	0.031	0.014	0.017	0.010	0.005
Cr^{3+}	0.000	0.000	0.000	0.000	0.000	0.001	0.000	0.000
Fe^{3+}	0.204	0.248	0.360	0.398	0.633	0.775	0.787	0.873
Fe^{2+}	0.339	0.299	0.204	0.189	0.087	0.060	0.145	0.058
Mn^{2+}	0.032	0.033	0.030	0.032	0.003	0.000	0.000	0.000
Mg^{2+}	0.423	0.405	0.383	0.357	0.249	0.136	0.014	0.039
Ca^{2+}	0.822	0.749	0.614	0.566	0.295	0.140	0.003	0.046
Na^+	0.170	0.244	0.381	0.425	0.691	0.845	0.959	0.945
K^+	0.000	0.000	0.000	0.002	0.003	0.000	0.001	0.000

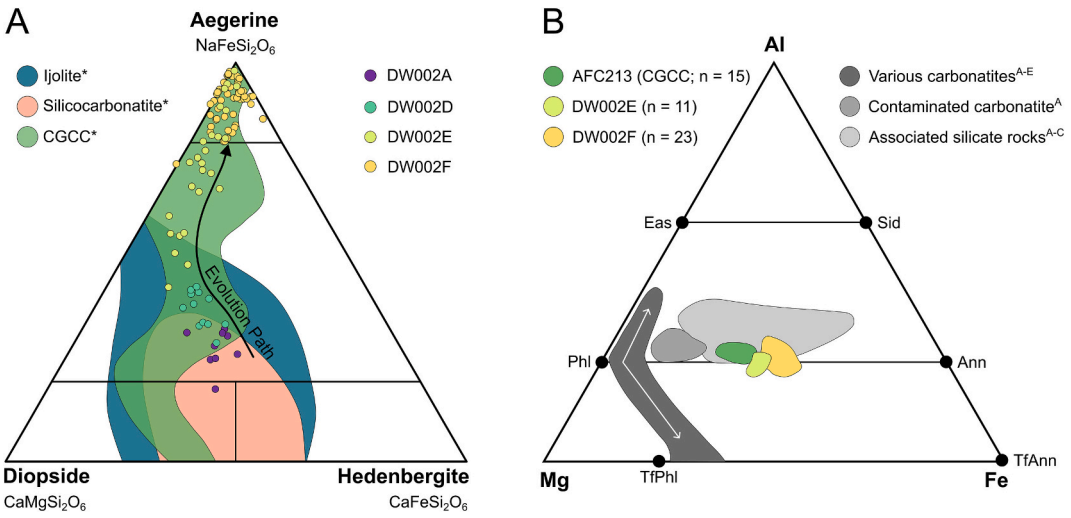

Fig. 9. Ternary diagrams showing clinopyroxene, mica and garnet compositions with comparable data.
A) Clinopyroxene composition shown by mole% of diopside, hedenbergite and aegirine. Clinopyroxene of the xenolith profile (with euhedral and anhedral differentiation where possible) are compared to clinopyroxenes of ijolites, nepheline silicocarbonatites and CGCC (*Cooper and Reid, 1998).
B) Mica composition based on Mg, Al and Fe_{Total} contents in apfu (atoms per formula unit). For comparison, compiled fields of carbonatites, silica-contaminated carbonatites and associated silicate rocks of other carbonatite complexes ([A]Kaiserstuhl Volcanic Complex, Braunger et al., 2018; Giebel et al., 2019a; [B]Jacupiranga Complex, Brod et al., 2001; [C]Palabora Complex, Giebel et al., 2019b; [D]Kovdor Complex, Krasnova et al., 2004; [E]Sokli Complex, Lee et al., 2003) are shown. *Please note that the mica compositions for Dicker Willem are derived from normalised, semi-quantitative µXRF data. Therefore, they should be considered as good approximation, though not as precise as EPMA data.*

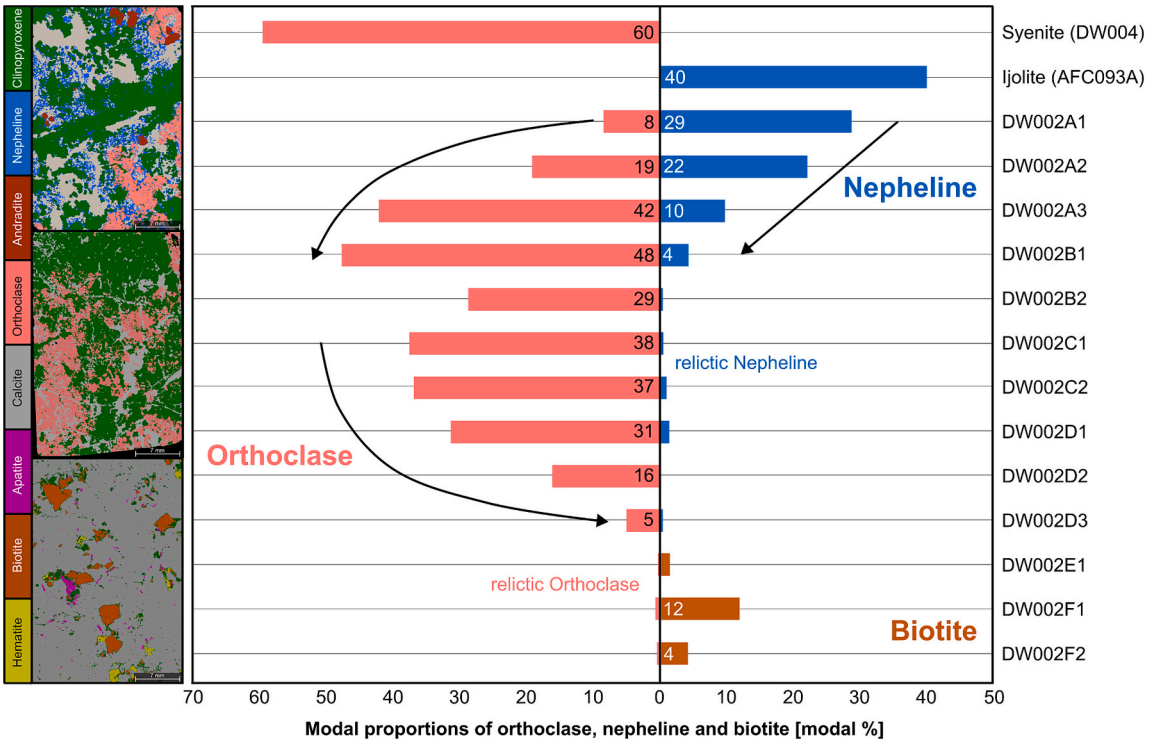

Fig. 10. Modal proportions of K-feldspar (red bars), nepheline (blue bars) and biotite (orange) in samples DW002A1–DW002F2 compared to ijolite (AFC93A) and syenite (DW004). Arrows indicate trends between orthoclase, nepheline and biotite proportions in the studied samples along the xenolith profile. Micro-XRF elemental maps from three representative thin sections of the xenolith's center to the endocontact (DW002A, DW002C and DW002F) showing the change in mineralogy and texture. (For interpretation of the references to colour in this figure legend, the reader is referred to the web version of this article.)

Similar biotite-rich reaction fringes around xenoliths in contact with carbonatitic magma are known from many localities (e.g., Giebel et al., 2019b; Viladkar, 2015; Vuorinen and Skelton, 2004). Further, biotite composition in the investigated samples is atypical for uncontaminated carbonatites, which typically crystallize very Fe-poor phlogopite (Brod et al., 2001; Chmyz et al., 2025), but similar to cases, where mica formed by silicate wall-rock assimilation (Fig. 9B; Giebel et al., 2019b and references therein). In this sense, the occurrence and composition of biotite is in line with formation by interaction between the investigated xenolith and carbonatite magma.

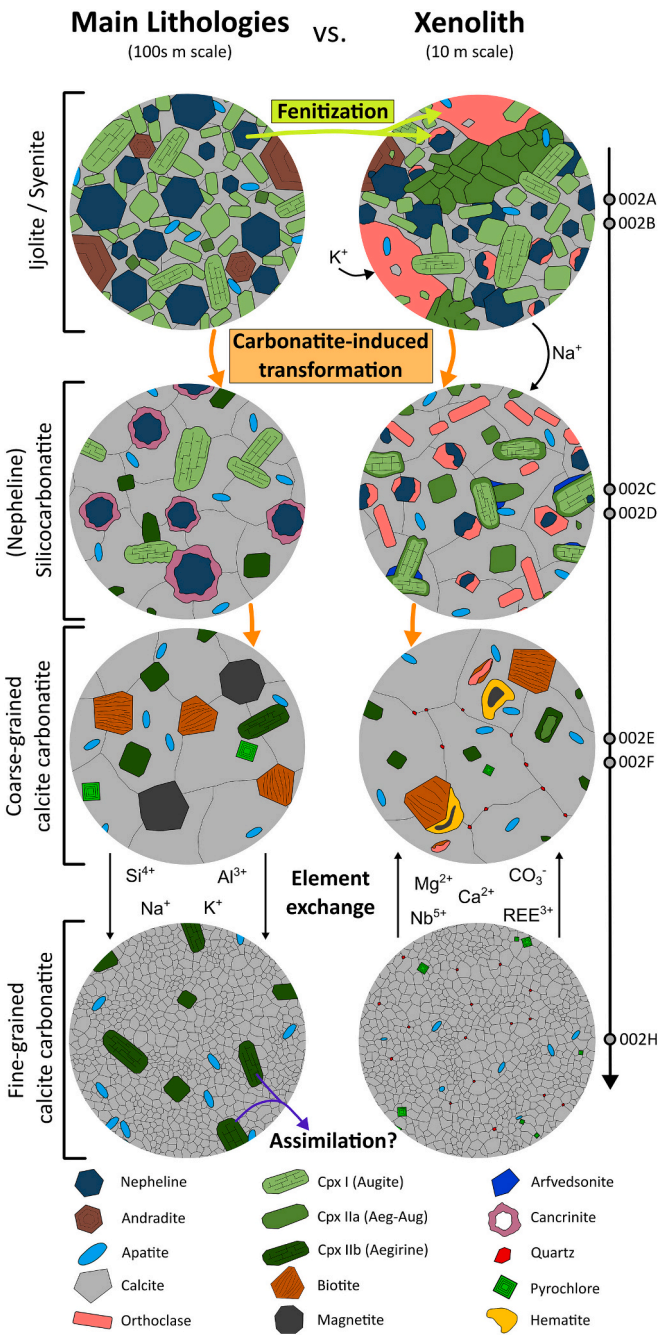

Fig. 11. A schematic representation depicting the mineral and textural composition of the Dicker Willem lithologies, including the studied xenolith. The illustration outlines the processes contributing to their formation.

Inversion of the orthoclase abundance-trend (Fig. 10) most likely marks the transition between the dominant influence of fenitizing carbohydrothermal fluids (orthoclase formation) and the surrounding carbonatite magma (orthoclase resorption and biotite formation). Texturally, similarly sized subhedral to euhedral recrystallized feldspar and clinopyroxene (DW002C and E) are consistent with experimental results indicating that clinopyroxene and K-feldspar can co-crystallize within a narrow temperature range of 725–750 °C (Stabile et al., 2021) suggesting increasingly magmatic conditions. Other features, such as biotite formation and cancrinitization of nepheline are typical for interaction with carbonatite magma (Giebel et al., 2019b; Harmer, 1999; Ladisic et al., 2025). Accordingly, the textures in orthoclase-free ijolite (e.g., samples AFC269A & C; Fig. 3G-H) show that nepheline in contact with calcite rather forms cancrinite, which can be described by the following reaction (3; Edgar, 1963):

nepheline + carbonatite melt → cancrinite.

$$6\,NaAlSiO_4 + 2\,CaCO_3 + 2\,H_2O \rightarrow Na_6Ca_2\left[(CO_3)_2\,|Al_6Si_6O_{24}\right]\cdot 2H_2O \quad (3)$$

The breakdown of nepheline to cancrinite and calcite was experimentally determined to occur in the range of 770–950 °C and X_{CO2} of 0.8–0.3 at 2 kbar, although strongly dependent on water availability (Sirbescu and Jenkins, 1999). Henderson and Ezepue (1989) estimated 750–900 °C for cancrinite-bearing phonolites at 1 kbar, while Sobolev et al. (1974) reported 630 °C at 1.1–1.5 kbar. Though these conditions differ from carbonatitic systems, they support a magmatic temperature regime at pressures matching Dicker Willem's subvolcanic emplacement. The high solubility of water in carbonatitic melts, up to nearly 10 wt% (Keppler, 2003), would provide sufficient water to facilitate cancrinite formation. We interpret these cancrinite bearing samples of nepheline silicocarbonatite, to reflect the interaction between ijolite and carbonatite melt rather than with carbohydrothermal fluids, in line with observations from elsewhere (e.g., Savard and Mitchell, 2021).

We suggest that the transformation of the xenolith reflects two subsequent processes: (1) initial carbohydrothermal fenitization of precursor calcite-bearing ijolites, followed by (2) subsequent carbonatization through resorption and replacement by carbonatite magma, partly overprinting precursor fenitization.

7.4. Isotopic and elemental dynamics of ijolite-carbonatite interaction

During the transformation of the large xenolith, both elemental and isotopic changes occur owing to the dynamic mixing of the chemical compositions of ijolite and carbonatite melts. This transformation, which spans various rock types, requires a significant flux of elements, involving both enrichment and depletion. The primary framework of this change is established by the transfer of Mg and Ca to the ijolitic silicate rock and the depletion of Si and Al (Table 2). As previously mentioned, the metasomatism associated with carbonatite is interpreted to be potassic, while Na is thought to originate from dissolved nepheline. This results in a counterflow of these two alkalis within the xenolith, with both being depleted closer to the contact with the melt.

The presence of a ferroan dolomite reaction fringe surrounding the xenolith (Fig. 2D) can be attributed to locally elevated magnesium activity, which facilitated dolomite formation (Chakhmouradian et al., 2016). The substantial enrichment of Nb in the immediate surrounding rock of the xenolith (around 2800 ppm) compared to levels <100 ppm (Table 2) aligns with a recent study that links the formation and solubility of pyrochlores in carbonatite melts directly to Si availability (Sun and Yaxley, 2025). The relative enrichment of REE in the outer sections of the xenoliths may be controlled by the flux of alkalis and silica, as demonstrated by experiments (Anenburg et al., 2020).

Carbon and oxygen isotope ratios of both the large xenolith and the FGCC evolve towards higher values from the primary igneous carbonatite field along trends of contamination or high-temperature fractionation (Deines, 1989). While contamination of the carbonatitic melt by the gneissic basement could plausibly explain the elevated O ratios, a carbonate-bearing source for elevated C ratios is absent. Therefore, Rayleigh fractionation appears to be the more plausible mechanism for explaining the elevated C and O ratios of the FGCC.

No evidence of "antiskarn formation" (sensu Anenburg and Mavrogenes, 2018) or direct silicate mineralization was observed at the immediate contact with the xenolith. Instead, the xenolith is encased in flow-banded carbonatite, indicating that the surrounding magma remained dynamic and molten before final solidification. These conditions likely allowed for prolonged thermal exchange and chemical transformation of the xenolith. The prolonged molten state may have enabled the migration of elements away from the xenolith, either through mixing or by the settling and accumulation of "antiskarn

minerals" elsewhere in the system. Supporting evidence throughout Dicker Willem are cumulate layers or aggregates of macrocrysts in the fine-grained calcite carbonatite, such as biotite, aegirine, pyrochlore, dolomite or magnetite (Cooper, 1988; Reid and Cooper, 1992).

7.5. An alternative way to form (silico)carbonatites

Nepheline silicocarbonatites at Dicker Willem seem to be limited to a few occurrences in the CGCC, often in immediate vicinity of ijolite (Fig. 1). As sample sets from these locations (AFC093A-F, AFC267A-C, AFC268A-B, AFC269A-C) also show a gradual transition from ijolite to nepheline silicocarbonatite, we assume that the nepheline silicocarbonatites are the results of ijolite transformation by carbonatitic magma and are not the remains of a primary magma from which ijolite and coarse-grained calcite carbonatites are derived (Cooper and Reid, 1998).

The outer part of the xenolith closely resembles a coarse-grained calcite carbonatite (Fig. 11). The grain size of calcite, the composition of clinopyroxene (aegirine), biotite and whole rock elemental signatures are nearly indistinguishable to those of the CGCC. Oxygen isotope thermometry (Deines, 1989; Reid and Cooper, 1992) indicates magmatic temperatures (>800 °C) for magnetite-clinopyroxene pairs, while lower temperatures (~600 °C) recorded by biotite-magnetite and biotite-clinopyroxene pairs suggest late-stage biotite formation during rock-magma interaction. Given the overlapping isotopic signatures (C, O, Nd, Sr, Pb) of the ijolite, silicocarbonatite, and CGCC (Reid and Cooper, 1992; Reid and Cooper, 1998), even the CGCC domains, or what appear to be xenoliths in the FGCC (Fig. 1), may represent extensively replaced ijolitic precursors. Smaller xenoliths have been completely transformed into CGCC (Fig. 2E), while nepheline silicocarbonatites likely represent intermediate stages of this process (Figs. 3H & 4F). This suggests that the entire CGCC unit could be a product of carbonatite-driven transformation, with silicate-rich domains acting as relicts of the original ijolitic rock, gradually transitioning into silicocarbonatite and, ultimately, more evolved CGCC. A schematic cross-section of this process is illustrated in Fig. 12. While this model aligns with existing geochemical data from Dicker Willem, it challenges the traditional

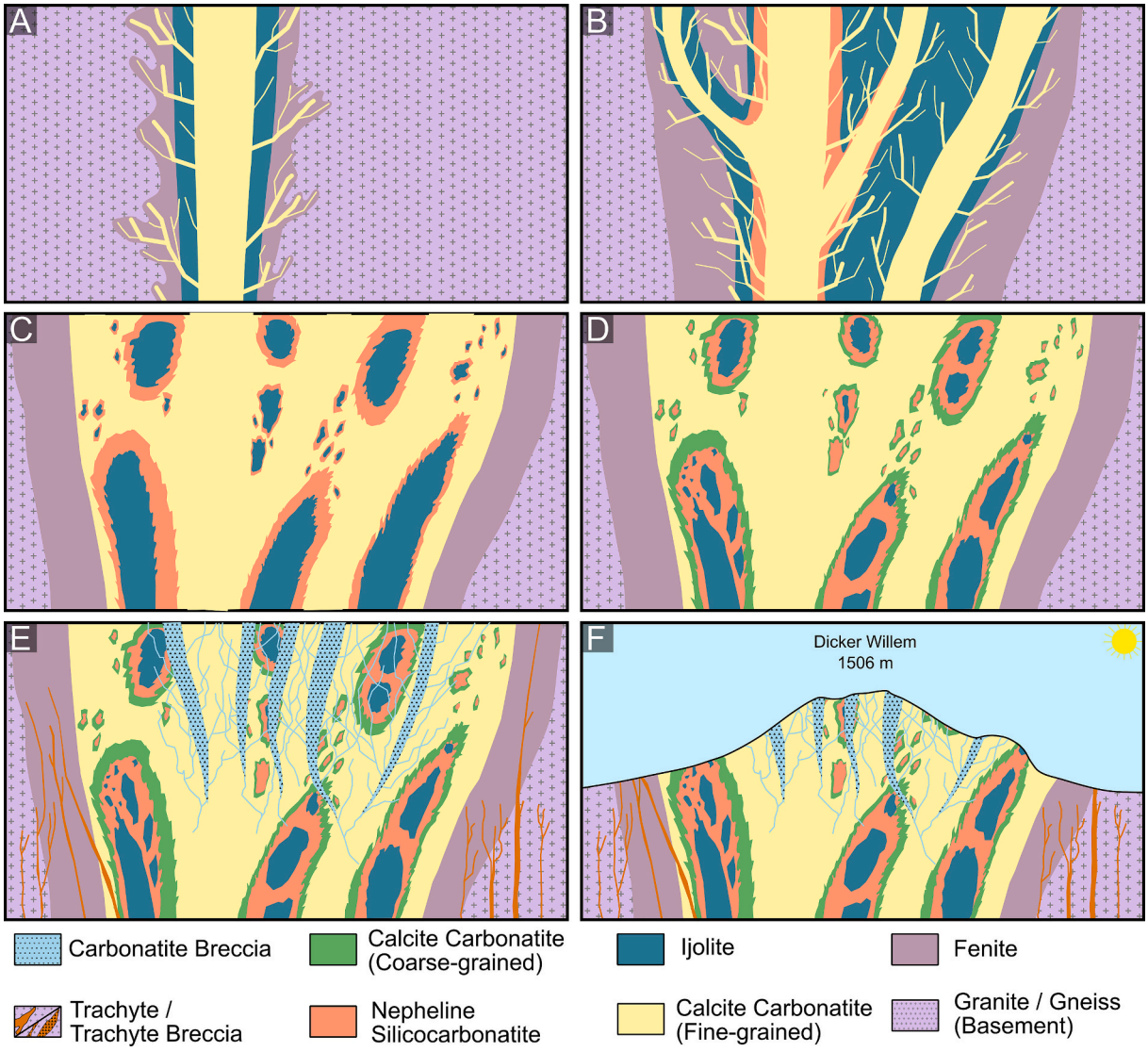

Fig. 12. Schematic representation of the proposed emplacement sequence of the Dicker Willem Complex modified after Cooper (1988). A) Initial carbonatite pulse interacts with granitic to gneissic country rock, inducing carbonate magma metasomatism/melting, forming ijolite and fenite, and consuming the carbonate melt. B) Subsequent pulses of carbonatitic magma generate additional interaction products. C) Later stages involve major carbonatite intrusions disrupting earlier ijolitic bodies, initiating a second phase of magmatic and metasomatic interaction and forming a silicocarbonatite zone. D) Intensified interaction further modifies the ijolites, resulting in the creation of coarse-grained calcite carbonatite. E) Late-stage fractionated carbonatite breccia intrudes the center, accompanied by peripheral trachyte. F) Current exposure of the Dicker Willem Complex along an N-S profile.

cumulate formation hypothesis from a silicocarbonatitic parental melt (Cooper and Reid, 1998; Reid and Cooper, 1998).

While the spatial extent of carbonatite-induced melting at Dicker Willem remains uncertain, this process likely plays a critical role in the formation of silicocarbonatites and even carbonatites. However, its broader significance for other carbonatite complexes is still unclear.

At the Fen complex (Norway), melteigite and calcite melteigite (hollaite) are closely associated with carbonatite (Savard and Mitchell, 2021), displaying clinopyroxene compositional trends similar to those observed in Dicker Willem xenoliths (Cooper and Reid, 1998; this study). Similarly, at the Prairie Lake complex (Canada), ijolites, calcite ijolites (hollaites), malignites, and carbonatites occur together (Savard and Mitchell, 2021). Despite minor variations, the mineralogical relationships between ijolite-series rocks, syenitic rocks (including malignites and foid syenites), silicocarbonatites (including hollaites), and carbonatites appear consistent across these complexes. Further research is needed to assess whether these occurrences share a magmatically transformed origin.

Commonly proposed models to explain the formation of silicocarbonatites include (1) direct precipitation from SiO_2-bearing carbonate melts or CO_2-bearing silicate melts (prior to potential immiscibility) and (2) products of contamination of carbonatitic melts by silicate wall-rock material (e.g., Anenburg and Walters, 2024; Cooper and Reid, 1998; Giebel et al., 2019b; Moore et al., 2022; Savard and Mitchell, 2021). The present study introduces an additional mechanism: magmatic transformation of silicate rocks by carbonatite magma, involving in-situ dissolution-reprecipitation of silicates and the resorption and displacement of original mineral phases. This model may help resolve previous contradictions regarding the genesis of the association between silicate rocks, silicocarbonatites and carbonatites.

8. Conclusions

The present study offers new perspectives on the interaction between silicate rocks and carbonatitic magma. It shows that a former ijolite (composed of clinopyroxene, nepheline, and calcite) can gradually transform into coarse calcite carbonatite that is virtually identical to a "primary" calcite carbonatite. Within a 4-m radius, the xenolith initially adopts a more syenitic composition as nepheline is replaced by orthoclase, a process facilitated by carbonatite-derived carbohydrothermal fluids. However, this composition steadily shifts towards the interface with the carbonatite host rock to silicocarbonatite eventually consisting primarily of calcite while the early clinopyroxene and orthoclase are resorbed. In the fringe region, minor yet notable crystallization of biotite, aegirine, and magnetite occurs, resulting in a composition that closely resembles that of a coarse-grained calcite carbonatite previously documented at Dicker Willem.

The depletion of Si, Fe, K, Na, and Al in the xenolith, along with the enrichment of Ca, Sr, and REE as it approached the carbonatitic host rock, is consistent with the observed transformations. The composition of clinopyroxene also shifts from augite to aegirine as it increasingly incorporates Na, reflecting published clinopyroxene data for corresponding lithologies. Similarly, the stable isotope data of ijolite and coarse-grained calcite carbonatite are comparable, and isotope data from the literature (Nd, Sr, Pb) share the same signature, supporting a common origin for ijolites and coarse-grained calcite carbonatites.

Thus, this study demonstrates that a silicate rock in direct contact with calcite carbonatitic magma can progressively transform into a silicocarbonatitic or even a calcite carbonatitic rock through magmatic replacement. The formation of carbonatitic rocks represents a selectively applicable, alternative explanation for the occurrence of transitional nepheline silicocarbonatites and coarse-grained calcite carbonatites at Dicker Willem, suggesting they are products of intense interaction between precursor ijolites and numerous pulses of carbonatitic melt.

CRediT authorship contribution statement

Lorenz Kemmler: Writing – original draft, Visualization, Validation, Methodology, Investigation, Formal analysis, Data curation, Conceptualization. **R. Johannes Giebel:** Writing – review & editing, Supervision, Project administration, Methodology, Investigation, Funding acquisition, Conceptualization. **Benjamin F. Walter:** Writing – review & editing, Supervision, Project administration, Funding acquisition, Conceptualization. **Michael A.W. Marks:** Writing – review & editing, Supervision, Project administration, Funding acquisition. **David L. Reid:** Writing – review & editing, Validation, Resources. **Mohsin Raza:** Writing – review & editing, Data curation. **Tobias Kluge:** Writing – review & editing, Data curation. **Gregor Markl:** Writing – review & editing, Supervision, Project administration.

Declaration of competing interest

The authors declare that they have no known competing financial interests or personal relationships that could have appeared to influence the work reported in this paper.

Acknowledgements

Elisabeth Eiche, Janine Wagner, Maya Denker, and Claudia Mössner are sincerely thanked for their contributions to lab administration and assistance with the whole rock analyses. The authors, furthermore, express their gratitude to Alan Marlow (Shali group holdings (Pty) Ltd) for their valuable assistance during field work and area access permission, as well as Anna Nguno (Ministry of Mines and Energy, Windhoek, Namibia) for administrative and regulatory support. DLR wishes to acknowledge additional research funds provided by Phil Janney, Department of Geological Sciences, University of Cape Town. This study was supported by the DFG grants WA 3116/4-1, WA3116/14-1, MA 2563-25 and GI1499/5-1.

Appendix A. Supplementary data

Supplementary data to this article can be found online at https://doi.org/10.1016/j.lithos.2026.108485.

Data availability

The data underlying this article are available in the article and in its online supplementary data. Supplementary data to this article can be found online at XXX. Whole-rock geochemistry was supplemented by literature data from Reid and Cooper (1992), Reid and Cooper (1998) and Ogungbuyi (2020).

References

Al-Aasm, I.S., Taylor, B.E., South, B., 1990. Stable isotope analysis of multiple carbonate samples using selective acid extraction. Chem. Geol. Isotope Geosci. Sect. 80, 119–125.

Anenburg, M., Aslam, I.N., 2024. Calcite-saturated natrocarbonatites: composition, crystal morphology, and weathering. Volcanica 7, 813–833.

Anenburg, M., Guzmics, T., 2023. Silica is unlikely to be soluble in upper crustal carbonatite melts. Nat. Commun. Nat. Publ. Group 14, 942.

Anenburg, M., Mavrogenes, J.A., 2018. Carbonatitic versus hydrothermal origin for fluorapatite REE-Th deposits: experimental study of REE transport and crustal "antiskarn" metasomatism. Am. J. Sci. 318, 335–366.

Anenburg, M., Walters, J.B., 2024. Metasomatic ijolite, glimmerite, silicocarbonatite, and antiskarn formation: carbonatite and silicate phase equilibria in the system Na2O–CaO–K2O–FeO–MgO–Al2O3–SiO2–H2O–O2–CO2. Contrib. Mineral. Petrol. 179, 40.

Anenburg, M., Mavrogenes, J.A., Frigo, C., Wall, F., 2020. Rare earth element mobility in and around carbonatites controlled by sodium, potassium, and silica. Sci. Adv. 6, eabb6570. American Association for the Advancement of Science.

Barker, D.S., 2001. Calculated silica activities in carbonatite liquids. Contrib. Mineral. Petrol. 141, 704–709.

Baudrand, M., Aloisi, G., Lécuyer, C., Martineau, F., Fourel, F., Escarguel, G., Blanc-Valleron, M.-M., Rouchy, J.-M., Grossi, V., 2012. Semi-automatic determination of

the carbon and oxygen stable isotope compositions of calcite and dolomite in natural mixtures. Appl. Geochem. 27, 257–265.
Braunger, S., Marks, M.A.W., Walter, B.F., Neubauer, R., Reich, R., Wenzel, T., Parsapoor, A., Markl, G., 2018. The petrology of the Kaiserstuhl volcanic complex, SW Germany: the importance of metasomatized and oxidized lithospheric mantle for carbonatite generation. J. Petrol. 59, 1731–1762.
Brod, J.A., Gaspar, J.C., de Araújo, D.P., Gibson, S.A., Thompson, R.N., Junqueira-Brod, T.C., 2001. Phlogopite and tetra-ferriphlogopite from Brazilian carbonatite complexes: petrogenetic constraints and implications for mineral-chemistry systematics. J. Asian Earth Sci. 19, 265–296.
Brooker, R.A., Kjarsgaard, B.A., 2011. Silicate–carbonate liquid immiscibility and phase relations in the system SiO2–Na2O–Al2O3–CaO–CO2 at 0·1–2·5 GPa with applications to carbonatite genesis. J. Petrol. 52, 1281–1305.
Chmyz, L., Azzone, R.G., Ruberti, E., Marks, M.A.W., dos T.J.S., Santos, 2022. Olivines as probes into assimilation of silicate rocks by carbonatite magmas: unraveling the genesis of reaction rocks from the Jacupiranga alkaline-carbonatite complex, southern Brazil. Lithos 416–417, 106647.
Chakhmouradian, A.R., Reguir, E.P., Zaitsev, A.N., 2016. Calcite and dolomite in intrusive carbonatites. I. Textural variations. Mineral. Petrol. 110 (2), 333–360.
Chmyz, L., Azzone, R.G., Ruberti, E., Guarino, V., 2025. Wall rock assimilation in carbonatite magmas: textural, mineral and whole-rock geochemical signatures in the Jacupiranga complex, Brazil. Geochemistry 85, 126218.
Cooper, A.F., 1988. Geology of Dicker Willem, a subvolcanic carbonatite complex in south-west Namibia. Commun. Geol. Surv. South West Afr./Namibia 3–12.
Cooper, A.F., Reid, D.L., 1991. Textural evidence for calcite carbonatite magmas, Dicker Willem, Southwest Namibia. Geology 19, 1193–1196.
Cooper, A.F., Reid, D.L., 1998. Nepheline Sövites as parental magmas in carbonatite complexes: evidence from Dicker Willem, Southwest Namibia. J. Petrol. 39, 2123–2136.
Cooper, A.F., Reid, D.L., 2000. The association of potassic trachytes and carbonatites at the Dicker Willem complex, Southwest Namibia: coexisting, immiscible, but not cogenetic magmas. Contrib. Mineral. Petrol. 139, 570–583.
Deines, P., 1989. Stable isotpe variations in carbonatites. In: Bell, K. (Ed.), Carbonatites: Genesis and Evolution. Unwin Hyman, London, pp. 301–359.
Doroshkevich, A.G., Veksler, I.V., Klemd, R., Khromova, E.A., Izbrodin, I.A., 2017. Trace-element composition of minerals and rocks in the Belaya Zima carbonatite complex (Russia): implications for the mechanisms of magma evolution and carbonatite formation. Lithos 284–285, 91–108.
Edgar, A.D., 1963. Phase equilibrium studies in the system Di Ne Ab-H_2O with studies on the crystal chemistry of nephelines. The University of Manchester, United Kingdom. Ph.D. thesis,. 155p.
Elliott, H.A.L., et al., 2018. Fenites associated with carbonatite complexes: a review. Ore Geol. Rev. 93, 38–59.
Giebel, R.J., Marks, M.A.W., Gauert, C.D.K., Markl, G., 2019a. A model for the formation of carbonatite-phoscorite assemblages based on the compositional variations of mica and apatite from the Palabora carbonatite complex, South Africa. Lithos 324–325, 89–104.
Giebel, R.J., Parsapoor, A., Walter, B.F., Braunger, S., Marks, M.A.W., Wenzel, T., Markl, G., 2019b. Evidence for Magma–Wall rock interaction in carbonatites from the Kaiserstuhl Volcanic Complex (Southwest Germany). J. Petrol. 60, 1163–1194.
Gittins, J., Mitchell, R.H., 2023. The genesis of calcite and dolomite carbonatite-forming magma by liquid immiscibility: a critical appraisal. Geol. Mag. 160, 1463–1480.
Gresens, R.L., 1967. Composition-volume relationships of metasomatism. Chem. Geol. 2, 47–65.
Gudelius, D., Marks, M.W., Markl, G., Nielsen, T.F.D., Kolb, J., Walter, B., 2023. The origin of ultramafic complexes with melilitolites and carbonatites: a petrological comparison of the Gardiner (E Greenland) and Kovdor (Russia) intrusions. J. Petrol. 64, egad036.
Guzmics, T., Berkesi, M., Bodnar, R.J., Fall, A., Bali, E., Milke, R., Vetlényi, E., Szabó, C., 2019. Natrocarbonatites: a hidden product of three-phase immiscibility. Geology 47, 527–530.
Harmer, R.E., 1999. The petrogenetic association of carbonatite and alkaline magmatism: constraints from the Spitskop complex, South Africa. J. Petrol. 40, 525–548.
Harmer, R.E., Gittins, J., 1998. The case for primary, mantle-derived carbonatite magma. J. Petrol. 39, 1895–1903.
Henderson, C.M.B., Ezepue, M.J.M., 1989. Petrogenesis of the dyke suite from the Marangudzi alkaline igneous ring complex. Zimbabwe. Memoirs Geol. Soc. India 15, 83–116.
Keppler, H., 2003. Water solubility in carbonatite melts. Am. Mineral. 88, 1822–1824.
Kim, K.-T., Burley, B.J., 1971. Phase equilibria in the system $NaAlSi_3O_8$ – $NaAlSiO_4$ – H_2O up to 15 Kb. a theoretical discussion. Can. J. Earth Sci. 8, 549–557. NRC Research Press.
Kim, S.-T., Coplen, T.B., Horita, J., 2015. Normalization of stable isotope data for carbonate minerals: implementation of IUPAC guidelines. Geochim. Cosmochim. Acta 158, 276–289.
Kramm, U., 1994. Isotope evidence for ijolite formation by fenitization: Sr−Nd data of ijolites from the type locality Iivaara, Finland. Contrib. Mineral. Petrol. 115, 279–286.
Krasnova, N.I., Balaganskaya, E.G., Garcia, D., 2004. Kovdor — Classic phoscorites and carbonatites. In: Wall, F., Zaitsev, A.N., Treloar, P.J. (Eds.), Phoscorites and Carbonatites from Mantle to Mine. Mineralogical Society of Great Britain and Ireland, pp. 99–132.
Kresten, P., Morogan, V., 1986. Fenitization at the Fen complex, southern Norway. Lithos 19, 27–42.
Ladisic, A., Marks, M.A.W., Walter, B.F., Giebel, R.J., Beranoaguirre, A., Markl, G., 2025. Permo-Triassic magmatism in the Damaraland Igneous Province, NW Namibia: the Ondurakorume alkaline-carbonatite complex. Geochemistry 85, 126287.
Le Bas, M.J., 2008. Fenites associated with carbonatites. Can. Mineral. 46, 915–932.
Le Maitre, R.W., Streckeisen, A., Zanettin, B., Le Bas, M.J., Bonin, B., Bateman, P. (Eds.), 2002. Igneous Rocks: A Classification and Glossary of Terms. Cambridge University Press, Cambridge.
Lee, M.J., Garcia, D., Moutte, J., Lee, J.I., 2003. Phlogopite and tetraferriphlogopite from phoscorite and carbonatite associations in the Sokli massif, Northern Finland. Geosci. J. 7, 9–20.
Lee, W.-J., Wyllie, P.J., 1998. Processes of crustal carbonatite formation by liquid immiscibility and differentiation, elucidated by model systems. J. Petrol. 39, 2005–2013.
Macey, P.H., et al., 2022. A continental back-arc setting for the Namaqua belt: evidence from the Kakamas Domain. Geosci. Front. 13, 101408.
Marsh, J.S., 1975. The Luderitz Alkaline Province, South West Africa II: metasomatism and assimilation in the contact aureole of the Granitberg Foyaite complex. S. Afr. J. Geol. 78 (2), 225–233.
Martin, L.H.J., Schmidt, M.W., Mattsson, H.B., Guenther, D., 2013. Element partitioning between immiscible carbonatite and silicate melts for dry and H2O-bearing systems at 1–3 GPa. J. Petrol. 54, 2301–2338.
Mitchell, R.H., 2005. Carbonatites and carbonatites and carbonatites. Can. Mineral. 43, 2049–2068.
Mitchell, R.H., Gittins, J., 2022. Carbonatites and carbothermalites: a revised classification. Lithos 430–431, 106861.
Moore, K.R., Brady, A.E., Costanzo, A., 2022. Crystal-liquid segregation in silicocarbonatite magma leads to the formation of calcite carbonatite. J. Petrol. 63, egac056.
Nabyl, Z., et al., 2020. A window in the course of alkaline magma differentiation conducive to immiscible REE-rich carbonatites. Geochim. Cosmochim. Acta 282, 297–323.
Ogungbuyi, I.P., 2020. Geochemical and isotopic constraints on the source regions of phanerozoic carbonatites and associated alkaline rocks from the Zandkopsdrift complex of Namaqualand, South Africa, and the Marinkas Quellen, and Dicker Willem complexes in Namibia. University of Cape Town, South Africa. Unpublished PhD thesis, 277p.
Otto, J.W., Wyllie, P.J., 1993. Relationships between silicate melts and carbonate-precipitating melts in CaO-MgO-SiO2-CO2-H2O at 2 kbar. Mineral. Petrol. 48, 343–365.
Reid, D.L., 1991. Alkaline rocks in the Kuboos-Bremen igneous province, southern Namibia: the Kanabeam multiple ring complex. Commun. Geol. Surv. Namibia 7, 3–13.
Reid, D.L., Cooper, A.F., 1992. Oxygen and carbon isotope patterns in the Dicker Willem carbonatite complex, southern Namibia. Chem. Geol. Isotope Geosci. Sect. 94, 293–305.
Reid, D.L., Cooper, A.F., 1998. Carbonatite and Silicate Magmas at Dicker Willem, Southern Namibia: Their Origin and Source Region Characteristics. International Kimberlite Conference, Extended Abstracts, pp. 727–729.
Reid, D.L., Cooper, A.F., Rex, D.C., Harmer, R.E., 1990. Timing of post–Karoo alkaline volcanism in southern Namibia. Geol. Mag. 127, 427–433.
Ries, J.B., Fike, D.A., Pratt, L.M., Lyons, T.W., Grotzinger, J.P., 2009. Superheavy pyrite (δ^{34}Spyr > δ^{34}SCAS) in the terminal proterozoic nama group, southern Namibia: a consequence of low seawater sulfate at the dawn of animal life. Geology 37, 743–746.
Rubie, D.C., Gunter, W.D., 1983. The role of speciation in alkaline igneous fluids during fenite metasomatism. Contrib. Mineral. Petrol. 82, 165–175.
Samoilov, V.S., 1991. The main geochemical features of carbonatites. J. Geochem. Explor. 40, 251–262.
Savard, J.J., Mitchell, R.H., 2021. Petrology of ijolite series rocks from the Prairie Lake (Canada) and Fen (Norway) alkaline rock-carbonatite complexes. Lithos 396–397, 106188.
Schmidt, M.W., Giuliani, A., Poli, S., 2024. The origin of carbonatites—combining the rock record with available experimental constraints. J. Petrol. 65, egae105.
Sirbescu, M., Jenkins, D.M., 1999. Experiments on the stability of cancrinite in the system Na 2 O-CaO-Al 2 O 3 -SiO 2 -CO 2 -H 2 O. Am. Mineral. 84, 1850–1860.
Sobolev, V.S., Bazarova, T.Y., Kostyuk, V.P., 1974. Inclusions in the minerals of some types of alkaline rocks. In: Sørensen, H. (Ed.), The Alkaline Rocks. John Wiley & Sons, London, pp. 389–401.
Stabile, P., Arzilli, F., Carroll, M.R., 2021. Crystallization of peralkaline rhyolitic magmas: pre- and syn-eruptive conditions of the Pantelleria system. Comptes Rendus. Géosci. 353, 151–170.
Su, K., Zhang, S.-B., Li, Z.-X., Zhang, L., Liang, T., Du, Y., Li, L., 2023. When carbonatite met granite: a carbonatite magma- wall rock reaction origin for the Paleoproterozoic pyroxenite and syenite in Fengzhen, North China. Lithos 454–455, 107231.
Sun, W., Yaxley, G.M., 2025. The solubility of pyrochlore in carbonatite melts at crustal conditions. In: Paper Presented at the Goldschmidt 2025 Conference. (GOLDSCHMIDT).
Tappe, S., Mitchell, R., 2026. Revised IUGS terminology for carbonatites and carbothermalites (SSRN scholarly paper no. 6098293). In: Social Science Research Network. https://doi.org/10.2139/ssrn.6098293.
Taylor, H.P., Frechen, J., Degens, E.T., 1967. Oxygen and carbon isotope studies of carbonatites from the Laacher See District, West Germany and the Alnö District, Sweden. Geochim. Cosmochim. Acta 31, 407–430.
Vartiainen, H., Woolley, A.R., 1976. The petrography, mineralogy and chemistry of the fenites of the Sokli carbonatite intrusion, Finland. Geol. Surv. Finl. 280, 1–87.

Vasyukova, O.V., Williams-Jones, A.E., 2022. Carbonatite metasomatism, the key to unlocking the carbonatite-phoscorite-ultramafic rock paradox. Chem. Geol. 602, 120888.
Viladkar, S.G., 2015. Mineralogy and geochemistry of fenitized nephelinites of the Amba Dongar complex, Gujarat. J. Geol. Soc. India 85, 87–97.
Vuorinen, J.H., Skelton, A.D.L., 2004. Origin of silicate minerals in carbonatites from Alnö Island, Sweden: magmatic crystallization or wall rock assimilation? Terra Nova 16, 210–215.
Wallace, M.E., Green, D.H., 1988. An experimental determination of primary carbonatite magma composition. Nature 335, 343–346. Nature Publishing Group.
Walter, B., Giebel, R.J., Marlow, A., Siegfried, P., Marks, M., Markl, G., Palmer, M., Kolb, J., 2022. The Kieshöhe carbonatites of southwestern Namibia - the post-magmatic role of silicate xenoliths on REE mobilisation. Commun. Geol. Surv. Namibia 25.
Walter, B.F., Giebel, R.J., Steele-MacInnis, M., Marks, M.A.W., Kolb, J., Markl, G., 2021. Fluids associated with carbonatitic magmatism: a critical review and implications for carbonatite magma ascent. Earth Sci. Rev. 215, 103509.
Watkinson, D.H., Wyllie, P.J., 1971. Experimental study of the composition join $NaAlSiO_4$-$CaCO_3$-H_2O and the genesis of Alkalic Rock—Carbonatite Complexes. J. Petrol. 12 (2), 357–378.
Williams-Jones, A.E., Palmer, D.A.S., 2002. The evolution of aqueous–carbonic fluids in the Amba Dongar carbonatite, India: implications for fenitisation. Chem. Geol. 185, 283–301.
Yaxley, G.M., Anenburg, M., Tappe, S., Decree, S., Guzmics, T., 2022. Carbonatites: classification, sources, evolution, and emplacement. Annu. Rev. Earth Planet. Sci. Annu. Rev. 50, 261–293.
Yuan, X., Zhong, R., Xiong, X., Gao, J., Ma, Y., 2023. Transition from carbonatitic magmas to hydrothermal brines: continuous dilution or fluid exsolution? Sci. Adv. 9, eadh0458. American Association for the Advancement of Science.
Zhu, X., Anenburg, M., Liu, Y., 2025. Non-alkali metals titrate silica out of carbonatite melts into insoluble silicate minerals. Geochim. Cosmochim. 413, 78–90.